Journal of Control, Automation and Electrical Systems (2021) 32:326–355
https://doi.org/10.1007/s40313-020-00675-9

# Computational Approach For Real-Time Interval Type-2 Fuzzy Kalman Filtering and Forecasting via Unobservable Spectral Components of Experimental Data

**Daiana Caroline dos Santos Gomes**[1] · **Ginalber Luiz de Oliveira Serra**[2]

Received: 29 June 2020 / Revised: 1 October 2020 / Accepted: 21 November 2020 / Published online: 3 January 2021


**Abstract**
In this paper, a methodology for design of Kalman filter, using interval type-2 fuzzy systems, in discrete time domain, via spectral decomposition of experimental data, is proposed. The adopted methodology consists of recursive parametric estimation of local state space linear submodels of interval type-2 fuzzy Kalman filter for tracking and forecasting of the dynamics inherited to experimental data, using an interval type-2 fuzzy version of Observer/Kalman Filter Identification (OKID) algorithm. The partitioning of the experimental data is performed by interval type-2 fuzzy Gustafson–Kessel clustering algorithm. The interval Kalman gains in the consequent proposition of interval type-2 fuzzy Kalman filter are updated according to unobservable components computed by recursive spectral decomposition of experimental data. Results illustrate the efficiency of proposed methodology, as compared to other approach widely cited in the literature, for filtering and tracking the state variables of Lorenz's chaotic attractor in a noisy environment, and its applicability for adaptive and real-time forecasting the dynamic spread behavior of novel coronavirus 2019 (COVID-19) outbreak in state of Maranhão and Brazil.

**Keywords** Epidemiological data · Systems identification · Interval type-2 fuzzy systems · Kalman filtering · COVID-19

## 1 Introduction

In science and engineering is very common the solution of problems with stochastic nature such as prediction, separation and detection of signals in the presence of random noise (Mack and Habets 2020; Gomez-Garcia et al. 2020; Liu et al. 2019; Zhu et al. 2019). Kalman filter (KF) is the most well-known and used mathematical tool for stochastic estimation from noisy and uncertain measurements. It was proposed by Rudolph E. Kalman in 1960, who published his famous paper "A New Approach to Linear Filtering and Prediction Problem" (Kalman 1960), describing a recursive solution to discrete time linear filtering problem and becoming a standard approach for optimal estimation. Since the time of its introduction, the Kalman filter has been the subject of extensive research and applications in the fields of orbit calculation, target tracking, integrated navigation, dynamic positioning, sensor data fusion, microeconomics, control, modeling, digital image processing, pattern recognition, image segmentation and image edge detection and others. This broad interest in KF is due to its optimality, convenient form for online real-time processing, easy formulation and implementation (Serra 2018).

Fuzzy systems have been widely used for modeling (Wang and Wu 2019; Chin and Lin 2018; Kim et al. 2020a; Zhao and Lin 2019) and also for health area (Khodaei-Mehr et al. 2018; Pham and Berger 2011). The successful applications of fuzzy systems are due to its structure based on rules, where the antecedent propositions of the rules define fuzzy operation regions and the consequent describes a corresponding physical behavior in those regions, and its capability of approximate functions as well as treat nonlinearities and uncertainties (Serra 2012). Recently, type-2 fuzzy systems have been highlighted in several applications due to their better ability to deal with uncertain information (Evangelista and Serra 2019; Mendel 2019). A special case within the

✉ Ginalber Luiz de Oliveira Serra
ginalber@ifma.edu.br

Daiana Caroline dos Santos Gomes
daianagomes159@gmail.com

[1] Federal University of Maranhão, Av. dos Portugueses, 1966, Bacanga, São Luís, MA 65080-805, Brazil

[2] Federal Institute of Education, Science and Technology of Maranhão, Av. Getúlio Vargas, 04, Monte Castelo, São Luís, MA 65030-005, Brazil

study of type-2 fuzzy logic is the interval type-2 fuzzy sets that, by simplifying the membership functions assigned to the sets, define a footprint of uncertainty (FoU) in data processing, which is limited by upper and lower membership functions (Liang and Mendel 2000).

With the emergence caused by COVID-19 and its rapid spread to several countries, authorities around the world have been implemented plans for fighting transmission of the virus based on guidelines provided by the World Health Organization (WHO) (Ryu and Chun 2020; WHO 2020a, b). The impacts caused by COVID-19 pandemic have affected health, social, economic, political and cultural spheres, unprecedented in the recent worldwide history of epidemics (Chakraborty and Maity 2020). In view to the problems faced to COVID-19 crisis, researchers from all scientific areas have proposed new studies and contributions as an effort to fight and understand the coronavirus disease (Feng et al. 2020; Fishbane and Hirsch 2020; Sun et al. 2020; Brown et al. 2020; Huang et al. 2020; Kang et al. 2020). In these contexts, computational modeling applied to analysis of epidemiological data has received increasing interest from the scientific community, aiming to characterize the dynamic evolution of infectious diseases outbreak and also helping in its control and prevention (Deeba et al. 2020; Price et al. 2019; Korcinska et al. 2020; Chen et al. 2020; van Gaalen et al. 2017; Sloan et al. 2020; van de Kassteele et al. 2019; Chowell et al. 2020).

Associated to epidemiological data analysis, the proposal for adaptive and real-time modeling methodologies which take into account the processing of uncertainties inherited to these types of experimental data (underreportings, lack of information, incubation period of the virus, time to seek care and diagnosis) is still open. The proposed methodology, based on interval type-2 fuzzy Kalman filter, is useful for adaptive and real-time forecasting of uncertain experimental data. A new formulation of type-2 fuzzy version of Observer/Kalman Filter Identification (OKID) algorithm, is proposed, for updating, recursively, the consequent proposition of type-2 fuzzy Kalman filter using spectral components extracted from the experimental data. Interval fuzzy sets characterizing the antecedent of type-2 fuzzy Kalman filter inference system are estimated by, also proposed, a formulation of interval type-2 fuzzy version of Gustafson–Kessel clustering algorithm. Computational results of tracking the states of a nonlinear dynamic system with chaotic behavior in a noisy environment show the efficiency of proposed methodology as compared to other approach widely cited in the literature. Applicability of proposed methodology is illustrated through experimental results from real-time interval forecasting of the COVID-19's dynamic spread behavior in state of Maranhão and Brazil.

### 1.1 Related Works

In the last years, studies involving the integration of fuzzy systems and Kalman filters have been proposed in the literature (Pires and Serra 2019; Eyoh et al. 2018; Gil et al. 2019; Bouhentala et al. 2019; Hwang et al. 2019). In (Wang et al. 2020), fuzzy sets are combined with a novel trace optimization method based on extended Kalman filter with nested probabilistic–numerical linguistic information applied in tracking a maneuvering target. Based on limited and uncertain information from different sensors, the proposed methodology is able to merge this information and is efficient when applied in the problem of trace optimization of an unknown maneuvering target in Sichuan province in China. In (Asl et al. 2020), an optimization methodology of an adaptive unscented Kalman filter (UKF) is presented by means of an evolutionary fuzzy algorithm named fuzzy adaptive grasshopper optimization algorithm. The efficiency of the method is verified by application to different benchmark functions, such as a robotic manipulator and a servo-hydraulic system, performing better when compared to previous versions of UKF. In (Matía et al. 2019), a reformulation in the uncertainty representation in fuzzy Kalman filters (FKF) is proposed, to solve the problem of uncertainty propagation that occurred in other approaches present in the literature for the FKF. Trapezoidal possibility distributions is used to represent fuzzy variables, defining regions of possibility and impossibility in asymmetric sets, which contributes to model sensor's uncertainty with more accuracy. In (Yang et al. 2019), a strategy based on fuzzy logic control to treat pathological symptoms of movement disorder with higher performance is presented. A slowly varying hidden variable in a neural network is estimated using an unscented Kalman filter and is used as a feedback variable to enhance control performance. The presented design, with enhanced control performance and higher hardware efficiency, has significant potential for clinical treatment of movement disorders and opens a new perspective for the applications in the fields of neural control engineering and brain–machine interfaces. In (Benhamida et al. 2019), an improved model predictive direct torque control (MPDTC) based on an adaptive fuzzy logic modulator and an extended Kalman filter is introduced. The methodology consists of an adaptive fuzzy logic-based duty cycle vector modulation, and two voltage vectors (VV) instead of a single VV are applied during the whole control cycle to promote the torque control performance and reduce its undulations. Moreover, a design of an extended Kalman filter estimator for drive systems is proposed. Despite the extensive literature in this context, there are still many fields to be explored regarding the association of Kalman filters and fuzzy logic.

Several mathematical, computational and statistical methods have already been proposed and widely applied in the

prediction of infectious diseases worldwide (Rajaei et al. 2019; Watkins et al. 2020; Martins et al. 2018; He et al. 2018). In (Weng et al. 2020), a seasonal autoregressive integrated moving average (SARIMA) model was used to predict the incidence of Chlamydia Trachomatis (CT) infection in Shenzhen city, China. The proposed model breaks down the time series data corresponding to monthly cases of CT infection into behavioral patterns such as trend, seasonal and random, in order to understand the epidemiological behavior of the disease and obtain more accurate predictions. In (Koolhof et al. 2020), negative binomial regression models were developed to forecast human infections by Ross River virus (RRV), which is Australia's most epidemiologically important mosquito-borne disease. The model uses data from climatic, environmental and oceanographic variables in order to understand the factors associated with RRV transmission in epidemiologically important regions in the state of Victoria and to establish an early warning forecasting system. In (Hranac et al. 2019), ensemble niche models to predict spatiotemporally varying bat birthing to examine how birthing cycles of African fruit bats, molossid bats, and non-molossid microbats inform the spatiotemporal occurrence of Ebola Virus Disease (EVD) spillover. The model uses pool sparse data and predicted the risk of EVD spillover at locations of the two 2018 EVD outbreaks in the Democratic Republic of the Congo. In (Chowell et al. 2020), an ensemble model was introduced for sequential forecasting that weights a set of plausible models and use a frequentist computational bootstrap approach to evaluate its uncertainty. The feasibility of the approach was demonstrated using simple dynamic differential equation models and the trajectory of outbreak scenarios of the Ebola Forecasting Challenge, providing forecasting horizon of 1-4 weeks. In (Stocks et al. 2020), a novel multilayered dynamic transmission model is presented for hepatitis C virus HCV transmission within a people who inject drugs (PWID) population. The approach based on this model is able to estimate the number of undiagnosed PWIDs, the true incidence, the average time until diagnosis, the reproduction numbers and associated uncertainties, using routine surveillance data.

Recently, with the beginning of the COVID-19 epidemic outbreak, several researchers have proposed model-based data analysis approaches applied to novel Coronavirus 2019 (Zhong et al. 2020; Lin et al. 2020; Mohd and Sulayman 2020; Duan and Zhang 2020; Chintalapudi et al. 2020; Fredj and Chrif 2020). The objective of these studies is to characterize the evolution of pandemic in certain regions and, thus, to contribute for the requirements adopted to contain the contamination by virus and allocation of resources. In this sense, a mathematical model for forecasting the transmission dynamics of COVID-19 in Korea is proposed in (Kim et al. 2020b). The mathematical model is based on SEIR model (Susceptible–Exposed–Infectious–Recovered) and takes account the behavioral changes that were implemented in the population since local transmission began. The study is able to predict the final size and the timing of the end of the epidemic as well as the maximum number of isolated individuals using daily confirmed cases comparing epidemiological parameters between the national level and the Daegu/Gyeongbuk area. The study proposed in (Park et al. 2020) addresses the role of asymptomatic carriers in transmission poses challenges for control of the COVID-19 pandemic. A mathematical framework is used to evaluate expected effects of asymptomatic transmission on the basic reproduction number $R_0$ (i.e., the expected number of secondary cases generated by an average primary cases in a fully susceptible population) and the fraction of new secondary cases attributable to asymptomatic individuals. The proposed methodology models the viral spread using a renewal equation framework, which allows to model the current incidence of infected individuals as a function of previous incidence and how infectiousness of an infected individual varies over the course of their infection. This analysis shows that understanding the temporal course of asymptomatic transmission can be important for assessing the importance of this route of transmission and for disease dynamics. In (Kanagarathinam and Sekar 2020), a SEIR model for COVID-19 was developed to show the importance of estimation of reproduction number ($R_0$). The work is focused on predicting the 2019 Novel Coronavirus outbreak at the early stage in India based on estimation of reproduction number ($R_0$) and help to take active measures prior to the spread of 2019-nCoV disease. The data of daily newly infective cases in India have been used as samples to obtain the reproduction number. The maximum likelihood approach has been carried out to the distribution of $R_0$. In (Rustam et al. 2020), several supervised machine learning models are compared to predict the number of patients affected by COVID-19. The four standard forecast models were used: linear regression (LR), least absolute shrinkage and selection operator (LASSO), support vector machine (SVM) and exponential smoothing (ES). Three types of predictions are made by each of the models, such as the number of newly infected cases, the number of deaths and the number of recoveries in next 10 days.

Differently from aforementioned approaches and others ones found from the literature, the scope of this paper outlines the integration of Kalman filter and interval type-2 fuzzy systems for tracking and forecasting the COVID-19 dynamic spread behavior. The design of interval type-2 fuzzy Kalman filter, according to proposed methodology, is based on spectral unobservable components and uncertainty regions extracted from experimental data.

### 1.2 Contributions

The originality of proposed methodology is outlined by the following main contributions:

- Applicability for adaptive and real-time forecasting of uncertain experimental data;
- A new formulation of interval type-2 fuzzy version of Gustafson–Kessel clustering algorithm for estimating and shaping the interval fuzzy sets characterizing the antecedent proposition of type-2 fuzzy Kalman filter inference system;
- A new formulation of type-2 fuzzy version of Observer/Kalman Filter Identification (OKID) algorithm, for recursive updating the consequent proposition of type-2 fuzzy Kalman filter based on unobservable spectral components extracted from the experimental data.

## 2 Interval Type-2 Fuzzy Computational Model

In this section, the proposed methodology for designing the interval type-2 fuzzy Kalman filter computational model from experimental data is presented. Formulations for pre-processing the experimental data by spectral analysis, parametric estimation of interval type-2 fuzzy Kalman filter antecedent proposition, parametric estimation of interval type-2 fuzzy Kalman filter consequent proposition and its recursive updating mechanism are addressed.

### 2.1 Pre-Processing by Singular Spectral Analysis

The singular spectral analysis technique is a mathematical tool for analyzing and decomposing complex time series into simpler components within the original data. Such unobservable components have relevant characteristics about the corresponding time series behavior (Elsner 2002).

#### 2.1.1 Training step

Let the initial experimental data set referring to $p$ outputs of the dynamic system under analysis, with $N_b$ samples, given by:

$$\mathbf{Y} = [\mathbf{y}_1 \quad \mathbf{y}_2 \quad \dots \quad \mathbf{y}_{N_b}]^T, \quad \mathbf{Y} \in \mathbb{R}^{p \times N_b} \tag{1}$$

where $\mathbf{y}_k \in \mathbb{R}^p$, with $k = 1, \dots, N_b$, is the output vector of the dynamic system at instant of time $k$. From this initial data set, a trajectory matrix $\mathbf{H}$ is defined, for each of the dimensions of $\mathbf{Y}$, considering a set of $\rho$ delayed vectors with dimension $\delta$, which is an integer number defined by user with $2 \leq \delta \leq N_b - 1$ and $\rho = N_b - \delta + 1$, given by:

$$\mathbf{H} = \begin{bmatrix} y_1 & y_2 & y_3 & \cdots & y_\rho \\ y_2 & y_3 & y_4 & \cdots & y_{\rho+1} \\ \vdots & \vdots & \vdots & \ddots & \vdots \\ y_\delta & y_{\delta+1} & y_{\delta+2} & \cdots & y_{N_b} \end{bmatrix}, \quad \mathbf{H} \in \mathbb{R}^{\delta \times \rho} \tag{2}$$

and the covariance matrix $\mathbf{S}$ is obtained as follows:

$$\mathbf{S} = \mathbf{H}\mathbf{H}^T, \qquad \mathbf{S} \in \mathbb{R}^{\delta \times \delta} \tag{3}$$

Applying the singular value decomposition (SVD) procedure to matrix $\mathbf{S}$, is obtained a set of eigenvalues in decreasing order such that $\sigma^1 \geq \sigma^2 \geq \cdots \geq \sigma^\delta \geq 0$ with their respective eigenvectors $\boldsymbol{\phi}^1, \boldsymbol{\phi}^2, \dots, \boldsymbol{\phi}^\delta$. Considering $d = max\{\varsigma, \text{such that } \sigma^\varsigma > 0\}$, and $\mathbf{V}^\varsigma = \mathbf{H}^T\boldsymbol{\phi}^\varsigma/\sqrt{\sigma^\varsigma}$ with $\varsigma = 1, \dots, d$, the singular value decomposition of the trajectory matrix $\mathbf{H}$, can be rewritten as:

$$\mathbf{H} = \mathbf{H}^1 + \mathbf{H}^2 + \cdots + \mathbf{H}^d \tag{4}$$

where the matrix $\mathbf{H}^\varsigma|^{\varsigma=1,\dots,d}$ is elementary (it has rank equal to 1) and is given by:

$$\mathbf{H}^\varsigma = \sqrt{\sigma^\varsigma}\boldsymbol{\phi}^\varsigma\mathbf{V}^{\varsigma T}, \quad \mathbf{H}^\varsigma \in \mathbb{R}^{\delta \times \rho} \tag{5}$$

The regrouping of $\mathbf{H}^\varsigma|^{\varsigma=1,\dots,d}$ into $\xi$ linearly independent matrices terms $\mathbf{I}^j|^{j=1,\dots,\xi}$, such that $\xi \leq d$, results in

$$\mathbf{H} = \mathbf{I}^1 + \mathbf{I}^2 + \cdots + \mathbf{I}^\xi \tag{6}$$

The unobservable components $\alpha^j|^{j=1,\dots,\xi}$ extracted from experimental data, resulted from the matrices $\mathbf{I}^j|^{j=1,\dots,\xi}$, are given by:

$$\alpha_k^j = \begin{cases} \frac{1}{k}\sum_{\nu=1}^{k+1} I_{\nu,k-\nu+1}^j & 1 \leq k \leq \delta^* \\ \frac{1}{\delta^*}\sum_{\nu=1}^{\delta^*} I_{\nu,k-\nu+1}^j & \delta^* \leq k \leq \rho^* \\ \frac{1}{N_b-k+1}\sum_{\nu=k-\rho^*+1}^{N-\rho^*+1} I_{\nu,k-\nu+1}^j & \rho^* < k \leq N_b \end{cases} \tag{7}$$

where $\delta^* = \min(\delta, \rho)$, $\rho^* = \max(\delta, \rho)$ and $N_b = \delta + \rho - 1$.

#### 2.1.2 Recursive step

After the initialization of spectral analysis algorithm in the training step, the next steps will be repeated for each time

instant $k = N_b + 1, N_b + 2, \ldots$, as formulated in sequel. The value of $\rho$ is increased by:

$$\rho = k - \delta + 1 \tag{8}$$

The covariance matrix is updated, recursively, as follows:

$$\mathbf{S}_k = \mathbf{S}_{k-1} + \boldsymbol{\Upsilon}_k, \qquad \mathbf{S}_k \in \mathbb{R}^{\delta \times \delta} \tag{9}$$

where $\boldsymbol{\Upsilon}_k = \boldsymbol{\psi}_k \boldsymbol{\psi}_k^T \in \mathbb{R}^{\delta \times \delta}$ with $\boldsymbol{\psi}_k = \left[y_\rho, y_{\rho+1}, \ldots, y_k\right]^T \in \mathbb{R}^{\delta \times 1}$. Applying SVD procedure to covariance matrix $\mathbf{S}_k$, the set of eigenvalues and their respective eigenvectors are updated such that the dynamic system output $y_k$ can be rewritten by:

$$y_k = h_k^1 + h_k^2 + \cdots + h_k^d \tag{10}$$

where $h_k^\varsigma = \kappa_k^\varsigma \boldsymbol{\psi}_k^T \boldsymbol{\phi}_k^\varsigma$ such that $\kappa_k^\varsigma$ corresponds to the last element of the eigenvector $\boldsymbol{\phi}_k^\varsigma$. Finally, the regrouping of the terms $h_k^\varsigma|^{\varsigma=1,\ldots,d}$ in $\xi$ disjoint terms $I_k^j|^{j=1,\ldots,\xi}$, results in

$$y_k = I_k^1 + I_k^2 + \ldots + I_k^\xi \tag{11}$$

such that $I_k^j = \alpha_k^j$, with $j = 1, \ldots, \xi$ and $k = N_b + 1, N_b + 2, \ldots$, represents the samples of extracted unobservable components at instant $k$. The recursive singular spectral analysis, according to proposed methodology, is implemented as described in Algorithm 1.

**Algorithm 1:** Recursive Singular Spectral Analysis

**input** : $\mathbf{Y}, \delta, \xi$

**output**: $\alpha_k^j|^{j=1,\ldots,\xi}$

*%Training step*;

**Step 1**: Compute $\rho = N_b - \delta + 1$;

**Step 2**: Construct the trajectory matrix $\mathbf{H}$ - Eq. (2);

**Step 3**: Compute the covariance matrix $\mathbf{S}$ - Eq. (3);

**Step 4**: Apply the SVD method in the covariance matrix $\mathbf{S}$ and obtain the set of eigenvalues $\sigma^1 \geq \sigma^2 \geq \cdots \geq \sigma^\delta \geq 0$ with their respective eigenvectors $\boldsymbol{\phi}^1, \boldsymbol{\phi}^2, \ldots, \boldsymbol{\phi}^\delta$;

**Step 5**: Rewrite the SVD of the matrix $\mathbf{S}$ in the form of Eq. (4);

**Step 6**: Regroup the matrices $\mathbf{H}^\varsigma|^{\varsigma=1,\ldots,d}$ in $\xi$ linearly independent matrix terms $\mathbf{I}^j|^{j=1,\ldots,\xi}$ - Eq. (6);

**Step 7**: Compute the unobservable components $\alpha_k^j|^{j=1,\ldots,\xi}$ - Eq. (7);

*%Recursive step*;

**while** $k \geq N_b + 1$ **do**

  **Step 1**: Update $\rho$ - Eq. (8);

  **Step 2**: Update the covariance matrix $\mathbf{S}_k$ - Eq. (9);

  **Step 3**: Update the set of eigenvalues $\sigma_k^1 \geq \sigma_k^2 \geq \cdots \geq \sigma_k^\delta \geq 0$ with their respective eigenvectors $\boldsymbol{\phi}_k^1, \boldsymbol{\phi}_k^2, \ldots, \boldsymbol{\phi}_k^\delta$ applying the SVD method in $\mathbf{S}_k$;

  **Step 4**: Rewrite the sample $y_k$ in the form of Eq. (10);

  **Step 5**: Regroup the terms $h_k^\varsigma|^{\varsigma=1,\ldots,d}$ in $\xi$ disjoint terms $I_k^j|^{j=1,\ldots,\xi}$ - Eq. (11);

**end**

### 2.1.3 Recursive Estimation of Measurement Noise Covariance

The spectral components extracted by singular spectral analysis in section 2.1 that presents smaller eigenvalues are considered as residuals and they are used as data set for recursive estimation of measurement noise covariance $R$, inherited to experimental data. The initial covariance of measurement noise $v$, is given by:

$$R = \mathrm{E}(vv^T) = \frac{1}{N_b} \sum_{j=1}^{N_b} v_j v_j^T \tag{12}$$

where $N_b$ is the length of experimental data set to be used in training step for initial parameterization of interval type-2 fuzzy Kalman filter and $v$ is the spectral component $\alpha^j$ considered as residual. The recursive updating of covariance $R$, at instants of time $k = N_b + 1, N_b + 2, \ldots$, is given by:

$$R_k = \frac{k-1}{k} R_{k-1} + \frac{1}{k} v_k v_k^T \tag{13}$$

Once the covariance $R$ of the residual $v$ is computed, an adaptive factor $\mathcal{X}_k$, with $k = N_b+1, N_b+2, \ldots$, is proposed, to be used as weighting factor for implementing the recursive updating mechanism of interval type-2 fuzzy Kalman filter, as follows:

$$\begin{cases} \mathcal{X}_k = 1 & \text{for } R_k < 1 \\ \mathcal{X}_k = R_k^{-1} & \text{for } 1 \leq R_k \leq 1000 \\ \mathcal{X}_k = 1 \times 10^{-3} & \text{for } R_k > 1000 \end{cases} \tag{14}$$

The algorithm for recursive estimation of noise covariance $R$ and weighting factor $\mathcal{X}$, according to proposed methodology, is implemented as described in Algorithm 2.

## 2.2 Parametric Estimation of Interval Type-2 Fuzzy Kalman Filter

The adopted structure of interval type-2 fuzzy Kalman filter presents the $i|^{[i=1,2,\ldots,c]}$-th fuzzy rule, given by:

$$R^{(i)}: \text{ IF } \mathbf{Z}_k \text{ IS } \widetilde{W}^i \text{ THEN } \begin{cases} \widetilde{\mathbf{x}}_{k+1}^i = \widetilde{\mathbf{A}}_k^i \widetilde{\mathbf{x}}_k^i + \widetilde{\mathbf{B}}_k^i \mathbf{u}_k + \boldsymbol{\mathcal{X}}_k \widetilde{\mathbf{K}}_k^i \widetilde{\boldsymbol{\epsilon}}_k^i \\ \widetilde{\mathbf{y}}_k^i = \widetilde{\mathbf{C}}_k^i \widetilde{\mathbf{x}}_k^i + \widetilde{\mathbf{D}}_k^i \mathbf{u}_k \end{cases} \tag{15}$$

**Algorithm 2:** Recursive Estimation of Measurement Noise Covariance

**input** : $\alpha^j$

**output**: $\mathcal{X}_k$, $R_k$

*%Training step*;

Compute the initial measurement noise covariance $R$ - Eq. (12);

Compute the initial adaptive factor $\mathcal{X}_k$ - Eq. (14);

*%Recursive step*;

**while** $k \geq N_b + 1$ **do**

  Update $R_k$ - Eq. (13);

  Update $\mathcal{X}_k$ - Eq. (14);

**end**

with $n$-th order, $m$ inputs, $p$ outputs, where $\mathbf{Z}_k$ is the linguistic variable of the antecedent; $\widetilde{W}^i$ is the interval type-2 fuzzy set; $\widetilde{\hat{\mathbf{x}}}_k^i \in \mathbb{R}^n$ is the estimated interval states vector of the nonlinear dynamic system; $\widetilde{\hat{\mathbf{y}}}_k^i \in \mathbb{R}^p$ is the estimated interval output vector and $\mathbf{u}_k \in \mathbb{R}^m$ is the input signal. The matrices $\widetilde{\mathbf{A}}_k^i \in \mathbb{R}^{n\times n}$, $\widetilde{\mathbf{B}}_k^i \in \mathbb{R}^{n\times m}$, $\widetilde{\mathbf{C}}_k^i \in \mathbb{R}^{p\times n}$, $\widetilde{\mathbf{D}}_k^i \in \mathbb{R}^{p\times m}$ and $\widetilde{\mathbf{K}}_k^i \in \mathbb{R}^{n\times p}$ are, respectively, state matrix, input matrix, output matrix, direct transmission matrix and Kalman gain matrix, which are uncertain parameters that describe the dynamics of the nonlinear system within a region of uncertainty. The residual error $\widetilde{\boldsymbol{\epsilon}}_k^i$ for $i$-th rule is defined as $\widetilde{\boldsymbol{\epsilon}}_k^i = \mathbf{y}_k - \widetilde{\hat{\mathbf{y}}}_k^i$, where $\mathbf{y}_k \in \mathbb{R}^p$ is the real output of the dynamic system and $\widetilde{\hat{\mathbf{y}}}_k^i$ is the interval estimated output by $i$-th linear submodel, and the $\boldsymbol{\mathcal{X}}_k$ is the weighting factor, as formulated in section 2.1.3, which corresponding to the level of filtering to be applied by interval type-2 fuzzy Kalman filter on the experimental data.

The interval type-2 fuzzy Kalman filter approximates the dynamic behavior inherited to experimental data through the weighted sum of Kalman filters defined in the consequent proposition of type-2 fuzzy Kalman filter rules, according to normalized interval activation degrees, of each $i$-th rule, as follows:

$$\widetilde{\hat{\mathbf{x}}}_{k+1} = \sum_{i=1}^{c} \widetilde{\mu}_{\widetilde{W}^i}^i(\mathbf{Z}_k)\widetilde{\mathbf{A}}_k^i\widetilde{\hat{\mathbf{x}}}_k + \sum_{i=1}^{c} \widetilde{\mu}_{\widetilde{W}^i}^i(\mathbf{Z}_k)\widetilde{\mathbf{B}}_k^i\mathbf{u}_k + \sum_{i=1}^{c} \widetilde{\mu}_{\widetilde{W}^i}^i(\mathbf{Z}_k)\boldsymbol{\mathcal{X}}_k\widetilde{\mathbf{K}}_k^i\widetilde{\boldsymbol{\epsilon}}_k^i \tag{16}$$

$$\widetilde{\hat{\mathbf{y}}}_k = \sum_{i=1}^{c} \widetilde{\mu}_{\widetilde{W}^i}^i(\mathbf{Z}_k)\widetilde{\mathbf{C}}_k^i\widetilde{\hat{\mathbf{x}}}_k + \sum_{i=1}^{c} \widetilde{\mu}_{\widetilde{W}^i}^i(\mathbf{Z}_k)\widetilde{\mathbf{D}}_k^i\mathbf{u}_k \tag{17}$$

with $\widetilde{\mu}_{\widetilde{W}^i}^i(\mathbf{Z}_k) = \left[\underline{\mu}_{\widetilde{W}^i}^i(\mathbf{Z}_k), \overline{\mu}_{\widetilde{W}^i}^i(\mathbf{Z}_k)\right]$, where $\underline{\mu}_{\widetilde{W}^i}^i(\mathbf{Z}_k)$ and $\overline{\mu}_{\widetilde{W}^i}^i(\mathbf{Z}_k)$ corresponds to lower and upper activation degrees in $i$-th cluster, respectively, and $c$ is the number of rules of interval type-2 fuzzy Kalman filter, such that:

$$\sum_{i=1}^{c} \widetilde{\mu}_{\widetilde{W}^i}^i(\mathbf{Z}_k) = 1, \qquad \widetilde{\mu}_{\widetilde{W}^i}^i(\mathbf{Z}_k) \geq 0 \tag{18}$$

### 2.2.1 Parametric Estimation of Antecedent

The partitioning of experimental data implies to computing of operating regions and, necessarily, the number of rules of the interval type-2 fuzzy Kalman filter. An interval type-2 fuzzy version of Gustafson–Kessel clustering algorithm was proposed, which is formulated in the sequel.

Given the experimental data set $\mathbf{Z}$, previously collected, of size $n \times N_b$, choose the number of clusters $1 < c < N_b$; the initial interval partition matrix $\widetilde{\mathbf{U}}^{(0)} \in \mathbb{R}^{c\times N_b}$, the termination tolerance $\mathcal{E} > 0$ and the interval weighting exponent $\widetilde{m} = \left[\underline{m}, \overline{m}\right]$, where $\underline{m}$ and $\overline{m}$ correspond to, respectively, weighting exponent of upper and lower membership functions.

**Repeat** for $l = 1, 2, \ldots$

**Step 1** - Compute the centers of the clusters:

$$\widetilde{\mathbf{v}}^{i^{(l)}} = \frac{\sum_{k=1}^{N_b} \left(\widetilde{\mu}_{\widetilde{W}^i}^i(\mathbf{Z}_k)^{i^{(l-1)}}\right)^{\widetilde{m}} \mathbf{Z}_k}{\sum_{k=1}^{N_b} \left(\widetilde{\mu}_{\widetilde{W}^i}^i(\mathbf{Z}_k)^{(l-1)}\right)^{\widetilde{m}}}, \quad 1 \leq i \leq c \tag{19}$$

**Step 2** - Compute the covariance matrices of the clusters:

$$\widetilde{\mathbf{F}}^i = \frac{\sum_{k=1}^{N_b} \left(\widetilde{\mu}_{\widetilde{W}^i}^i(\mathbf{Z}_k)^{(l-1)}\right)^{\widetilde{m}} \left(\mathbf{Z}_k - \widetilde{\mathbf{v}}^{i^{(l)}}\right)\left(\mathbf{Z}_k - \widetilde{\mathbf{v}}^{i^{(l)}}\right)^T}{\sum_{k=1}^{N} \left(\widetilde{\mu}_{\widetilde{W}^i}^i(\mathbf{Z}_k)^{(l-1)}\right)^{\widetilde{m}}}, \quad 1 \leq i \leq c, \quad 1 \leq k \leq N_b \tag{20}$$

**Step 3** - Compute the distances:

$$\widetilde{D}_{k\widetilde{\mathbf{F}}^i}^i = \sqrt{\left(\mathbf{Z}_k - \widetilde{\mathbf{v}}^{i^{(l)}}\right)^T \left[\det\left(\widetilde{\mathbf{F}}^i\right)^{1/n} \left(\widetilde{\mathbf{F}}^i\right)^{-1}\right] \left(\mathbf{Z}_k - \widetilde{\mathbf{v}}^{i^{(l)}}\right)} \tag{21}$$

**Step 4** - Update the partition matrix:
If $\widetilde{D}_{k\widetilde{\mathbf{F}}^i}^i > 0$ for $1 \leq i \leq c$, $1 \leq k \leq N_b$

$$\widetilde{\mu}_{\widetilde{W}^i}^{i^{(l)}}(\mathbf{Z}_k) = \left[\underline{\mu}_{\widetilde{W}^i}^i(\mathbf{Z}_k), \overline{\mu}_{\widetilde{W}^i}^i(\mathbf{Z}_k)\right] \tag{22}$$

where

$$\underline{\mu}^{i(l)}_{\widetilde{W}^i}(\mathbf{Z}_k) = \min\left[\frac{1}{\sum_{j=1}^{c}\left(\underline{D}^i_{k\underline{\mathbf{F}}^i}/\underline{D}^i_{k\underline{\mathbf{F}}^i}\right)^{2/(\underline{m}-1)}}, \frac{1}{\sum_{j=1}^{c}\left(\overline{D}^i_{k\overline{\mathbf{F}}^i}/\overline{D}^i_{k\overline{\mathbf{F}}^i}\right)^{2/(\overline{m}-1)}}\right] \tag{23}$$

$$\overline{\mu}^{i(l)}_{\widetilde{W}^i}(\mathbf{Z}_k) = \max\left[\frac{1}{\sum_{j=1}^{c}\left(\underline{D}^i_{k\underline{\mathbf{F}}^i}/\underline{D}^i_{k\underline{\mathbf{F}}^i}\right)^{2/(\underline{m}-1)}}, \frac{1}{\sum_{j=1}^{c}\left(\overline{D}^i_{k\overline{\mathbf{F}}^i}/\overline{D}^i_{k\overline{\mathbf{F}}^i}\right)^{2/(\overline{m}-1)}}\right] \tag{24}$$

otherwise
$\widetilde{\mu}^{i(l)}_{\widetilde{W}^i}(\mathbf{Z}_k) = [0,\ 0]$ with $\underline{\mu}^{i(l)}_{\widetilde{W}^i}(\mathbf{Z}_k) \in [0,1]$ e $\overline{\mu}^{i(l)}_{\widetilde{W}^i}(\mathbf{Z}_k) \in [0,1]$
**Until** $\left\|\widetilde{\mathbf{U}}^{(l)} - \widetilde{\mathbf{U}}^{(l-1)}\right\| < \mathcal{E}$
The interval type-2 fuzzy Gustafson–Kessel clustering algorithm, according to proposed methodology, is implemented as described in Algorithm 3.

**Algorithm 3:** Interval Type-2 Fuzzy Gustafson–Kessel Clustering Algorithm

**input** : $\mathbf{Z}, \widetilde{m}, \mathcal{E}, \widetilde{\mathbf{U}}^{(0)}$
**output**: $\widetilde{\mathbf{U}}$
$l = 0$;
**repeat**
  $l = l + 1$;
  **for** $i = 1$ **to** $c$ **do**
    **Step 1**: Compute the centers of the clusters $\widetilde{\mathbf{v}}^{i(l)}$ - Eq. (19);
    **Step 2**: Compute the covariance matrices of the clusters $\widetilde{\mathbf{F}}^i$ - Eq. (20);
    **Step 3** - Compute the distances $\widetilde{D}^i_{k\widetilde{\mathbf{F}}^i}$ - Eq. (21);
    **Step 4**: Update the partition matrix $\widetilde{\mathbf{U}}^{(l)}$ - Eq. (22)-(24);
  **end**
**until** $\left\|\widetilde{\mathbf{U}}^{(l)} - \widetilde{\mathbf{U}}^{(l-1)}\right\| < \mathcal{E}$;

### 2.2.2 Parametric Estimation of Consequent

Once the interval type-2 fuzzy Kalman filter is obtained by black box modeling approach, it is necessary to estimate, from experimental data, the matrices that compose the interval type-2 fuzzy Kalman filter inference system consequent proposition, as formulated in Eq. (15). In this sense, an interval type-2 fuzzy OKID (Observer/Kalman Filter Identification) algorithm, is proposed. The interval type-2 membership values from partitions defined on experimental data, which were estimated by interval type-2 Gustafson–Kessel clustering algorithm, have been considered as weighting criteria for computing the consequent proposition of interval type-2 fuzzy Kalman filter inference system. The interval type-2 fuzzy OKID algorithm is formulated in the sequel.

Let the experimental data set $\mathbf{Z}$, such that $\mathbf{Z}_k = \begin{bmatrix}\mathbf{u}_k & \boldsymbol{\alpha}^*_k\end{bmatrix}^T$, where $\boldsymbol{\alpha}^*_k$ corresponds to spectral components extracted from the experimental data. Choose an appropriate number of Markov parameters $q$, through the following steps:
**Step 1** - Compute the matrix of regressors $\boldsymbol{\Lambda}$, given by:

$$\boldsymbol{\Lambda} = \begin{bmatrix} \mathbf{u}_q & \mathbf{u}_{q+1} & \cdots & \mathbf{u}_{N_b-1} \\ \mathbf{Z}_{q-1} & \mathbf{Z}_q & \cdots & \mathbf{Z}_{N_b-2} \\ \mathbf{Z}_{q-2} & \mathbf{Z}_{q-1} & \cdots & \mathbf{Z}_{N_b-3} \\ \vdots & \vdots & \ddots & \vdots \\ \mathbf{Z}_0 & \mathbf{Z}_1 & \cdots & \mathbf{Z}_{N_b-q-1} \end{bmatrix} \tag{25}$$

**Step 2** - Compute the interval observer Markov parameters $\widetilde{\overline{\mathbf{Y}}}^i$:

$$\mathbf{y}^T = \sum_{i=1}^{c} \widetilde{\boldsymbol{\Gamma}}^i \boldsymbol{\Lambda}^T \widetilde{\overline{\mathbf{Y}}}^{i^T} \tag{26}$$

where

$$\widetilde{\boldsymbol{\Gamma}}^i = \begin{bmatrix} \widetilde{\mu}^i_{\widetilde{W}^i}(\mathbf{Z}_q) & 0 & \cdots & 0 \\ 0 & \widetilde{\mu}^i_{\widetilde{W}^i}(\mathbf{Z}_{q+1}) & \cdots & 0 \\ 0 & 0 & \cdots & 0 \\ \vdots & \vdots & \ddots & \vdots \\ 0 & 0 & \cdots & \widetilde{\mu}^i_{\widetilde{W}^i}(\mathbf{Z}_{N_b-1}) \end{bmatrix} \tag{27}$$

is the diagonal weighting matrix of the $i$-th fuzzy rule obtained from the interval type-2 GK fuzzy clustering algorithm and

$$\begin{aligned}\widetilde{\overline{\mathbf{Y}}}^i &= \begin{bmatrix} \widetilde{\mathbf{D}}^i_k & \widetilde{\mathbf{C}}^i_k\widetilde{\overline{\mathbf{B}}}^i_k & \widetilde{\mathbf{C}}^i_k\widetilde{\overline{\mathbf{A}}}^i_k\widetilde{\overline{\mathbf{B}}}^i_k & \cdots & \widetilde{\mathbf{C}}^i_k\widetilde{\overline{\mathbf{A}}}^{i^{(q-1)}}_k\widetilde{\overline{\mathbf{B}}}^i_k \end{bmatrix} \\ &= \begin{bmatrix} \widetilde{\overline{\mathbf{Y}}}_0 & \widetilde{\overline{\mathbf{Y}}}_1 & \widetilde{\overline{\mathbf{Y}}}_2 & \cdots \widetilde{\overline{\mathbf{Y}}}_q \end{bmatrix}\end{aligned} \tag{28}$$

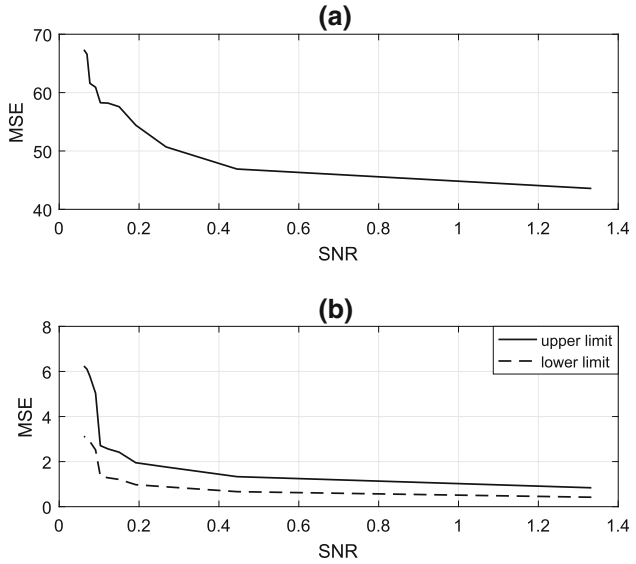


**Fig. 1** The MSE comparative analysis for filtering and tracking, based on 100 realizations, the state variable $x_1$ of Lorenz's chaotic attractor: **a** Approach in (Páramo-Carranza et al. 2017); **b** interval type-2 fuzzy Kalman filter based on proposed methodology

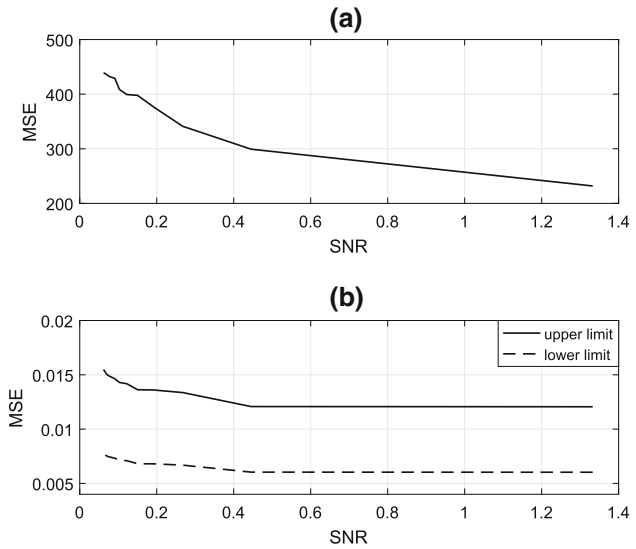


**Fig. 2** The MSE comparative analysis for filtering and tracking, based on 100 realizations, the state variable $x_2$ of Lorenz's chaotic attractor: **a** Approach in (Páramo-Carranza et al. 2017); **b** interval type-2 fuzzy Kalman filter based on proposed methodology

is the interval observer Markov parameters of $i$-th rule such that

$$\widetilde{\overline{\mathbf{A}}}_k^i = \left[\widetilde{\mathbf{A}}_k^i + \widetilde{\mathbf{K}}_k^i \widetilde{\mathbf{C}}_k^i\right] \tag{29}$$

$$\widetilde{\overline{\mathbf{B}}}_k^i = \left[\widetilde{\mathbf{B}}_k^i + \widetilde{\mathbf{K}}_k^i \widetilde{\mathbf{D}}_k^i \, , -\widetilde{\mathbf{K}}_k^i\right] \tag{30}$$

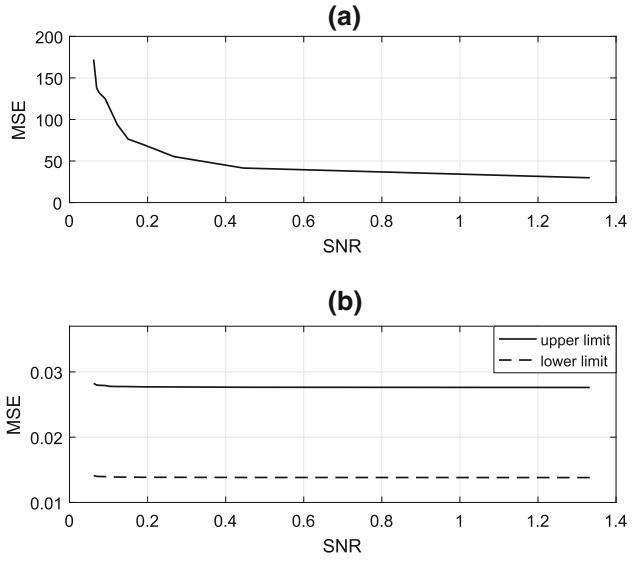


**Fig. 3** The MSE comparative analysis for filtering and tracking, based on 100 realizations, the state variable $x_3$ of Lorenz's chaotic attractor: **a** Approach in (Páramo-Carranza et al. 2017); **b** interval type-2 fuzzy Kalman filter based on proposed methodology

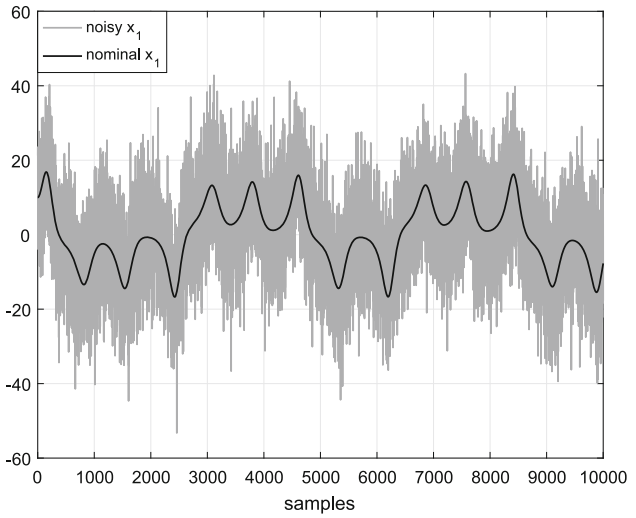


**Fig. 4** The computational data set of state variable $x_1$ from Lorenz's chaotic attractor corrupted by noise with $SNR = 0.65$

Manipulating Eq. (26):

$$\boldsymbol{\Lambda}\widetilde{\boldsymbol{\Gamma}}^i \mathbf{y}^T = \boldsymbol{\Lambda}\widetilde{\boldsymbol{\Gamma}}^i \boldsymbol{\Lambda}^T \widetilde{\overline{\mathbf{Y}}}^{i^T} \tag{31}$$

Assuming $\widetilde{\mathfrak{U}}^i = \boldsymbol{\Lambda}\widetilde{\boldsymbol{\Gamma}}^i \boldsymbol{\Lambda}^T$ and $\widetilde{\mathfrak{K}}^i = \boldsymbol{\Lambda}\widetilde{\boldsymbol{\Gamma}}^i \mathbf{y}^T$, Eq. (31) is rewriting as:

$$\widetilde{\mathfrak{U}}^i \widetilde{\overline{\mathbf{Y}}}^{i^T} = \widetilde{\mathfrak{K}}^i \tag{32}$$

Equation (32) is solved by QR factorization method, which is numerically robust since it avoids matrix inverse operations.

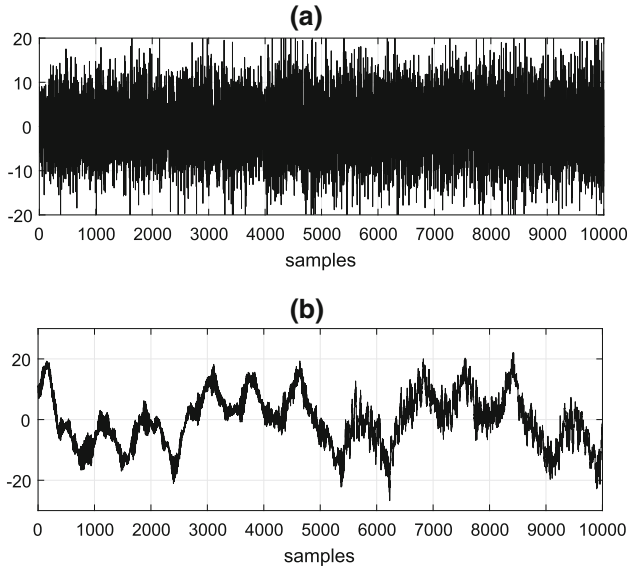


**Fig. 5** The temporal behavior of spectral components $\alpha^{j}|^{j=1,\ldots,2}$, which were extracted for state variable $x_1$ from Lorenz's chaotic attractor in a noisy environment with $SNR = 0.65$: **a** Unobservable component $\alpha^1$ assumed as residual; **b** Unobservable component $\alpha^2$ assumed as dynamically correlated to state variable $x_1$

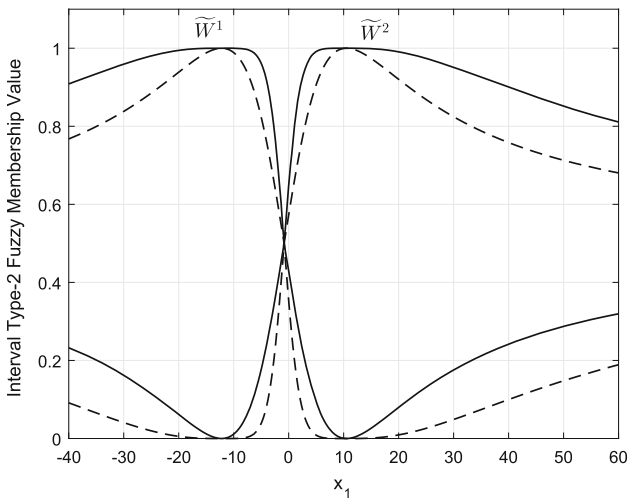


**Fig. 6** Interval type-2 fuzzy membership functions estimated by clustering of state variable $x_1$ from Lorenz's chaotic attractor

Applying QR factorization to the term $\widetilde{\mathfrak{U}}^i$ on the right side of the Eq. (32), it has:

$$\widetilde{\mathbf{Q}}^i \widetilde{\mathbf{R}}^i \widetilde{\widetilde{\mathbf{Y}}}^{i^T} = \widetilde{\widetilde{\mathbf{S}}}^i \tag{33}$$

where $\widetilde{\mathbf{Q}}^i$ is an orthogonal matrix, such that $\left(\widetilde{\mathbf{Q}}^i\right)^{-1} = \left(\widetilde{\mathbf{Q}}^i\right)^T$ and $\widetilde{\mathbf{R}}^i$ is an upper triangular matrix. Because the matrix $\widetilde{\mathbf{R}}^i$ is upper triangular, Eq. (33) can be solved by backward replacement, obtaining the observer's Markov parameter vector $\widetilde{\widetilde{\mathbf{Y}}}^i$.

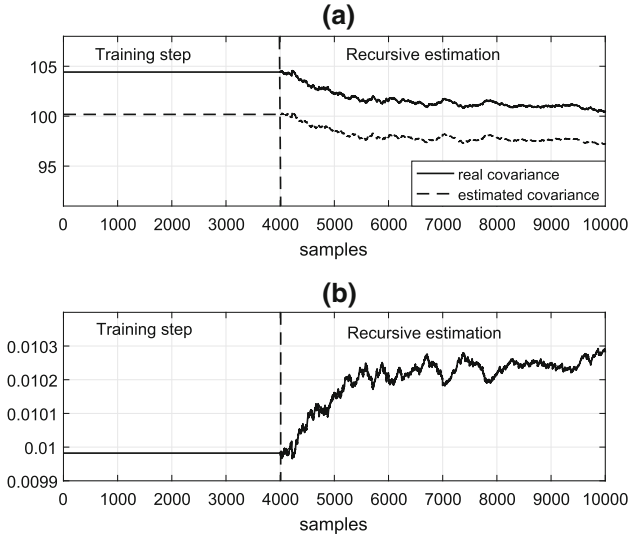


**Fig. 7** The temporal behavior of **a** measurement noise covariance $R_k$ associated to state variable $x_1$ and **b** the weighting factor $\boldsymbol{\chi}_k$ used for implementing the recursive updating mechanism of interval type-2 fuzzy Kalman filter

**Step 3** - Compute the observer gain and system Markov parameters:

$$\widetilde{\widetilde{\mathbf{Y}}}_0^i = \widetilde{\mathbf{D}}_k^i \tag{34}$$

$$\widetilde{\widetilde{\mathbf{Y}}}_j^i = \widetilde{\mathbf{C}}_k^i \widetilde{\widetilde{\mathbf{A}}}^{i^{(j-1)}} \widetilde{\widetilde{\mathbf{B}}}_k^i \tag{35}$$

$$= \left[ \widetilde{\mathbf{C}}_k^i \left( \widetilde{\mathbf{A}}_k^i + \widetilde{\mathbf{K}}_k^i \widetilde{\mathbf{C}}_k^i \right)^{(j-1)} \left( \widetilde{\mathbf{B}}_k^i + \widetilde{\mathbf{K}}_k^i \widetilde{\mathbf{D}}_k^i \right) , \right.$$
$$\left. -\widetilde{\mathbf{C}}_k^i \left( \widetilde{\mathbf{A}}_k^i + \widetilde{\mathbf{K}}_k^i \widetilde{\mathbf{C}}_k^i \right)^{(j-1)} \widetilde{\mathbf{K}}_k^i \right] \tag{36}$$

$$= \left[ \widetilde{\widetilde{\mathbf{Y}}}_j^{i^{(1)}} , \; -\widetilde{\widetilde{\mathbf{Y}}}_j^{i^{(2)}} \right], \quad j = 1, 2, 3, \ldots \tag{37}$$

Thus, the system Markov parameters are obtained as follows:

$$\widetilde{\mathbf{Y}}_0^i = \widetilde{\widetilde{\mathbf{Y}}}_0^i = \widetilde{\mathbf{D}}_k^i \tag{38}$$

$$\widetilde{\mathbf{Y}}_j^i = \widetilde{\widetilde{\mathbf{Y}}}_j^{i^{(1)}} - \sum_{\iota=1}^{j} \widetilde{\widetilde{\mathbf{Y}}}_j^{i^{(2)}} \widetilde{\mathbf{Y}}_{j-\iota}^i, \quad \text{for} \;\; j = 1, \ldots, q \tag{39}$$

$$\widetilde{\mathbf{Y}}_j^i = -\sum_{\iota=1}^{q} \widetilde{\widetilde{\mathbf{Y}}}_j^{i^{(2)}} \widetilde{\mathbf{Y}}_{j-\iota}^i, \quad \text{for} \;\; j = q+1, \ldots, \infty \tag{40}$$

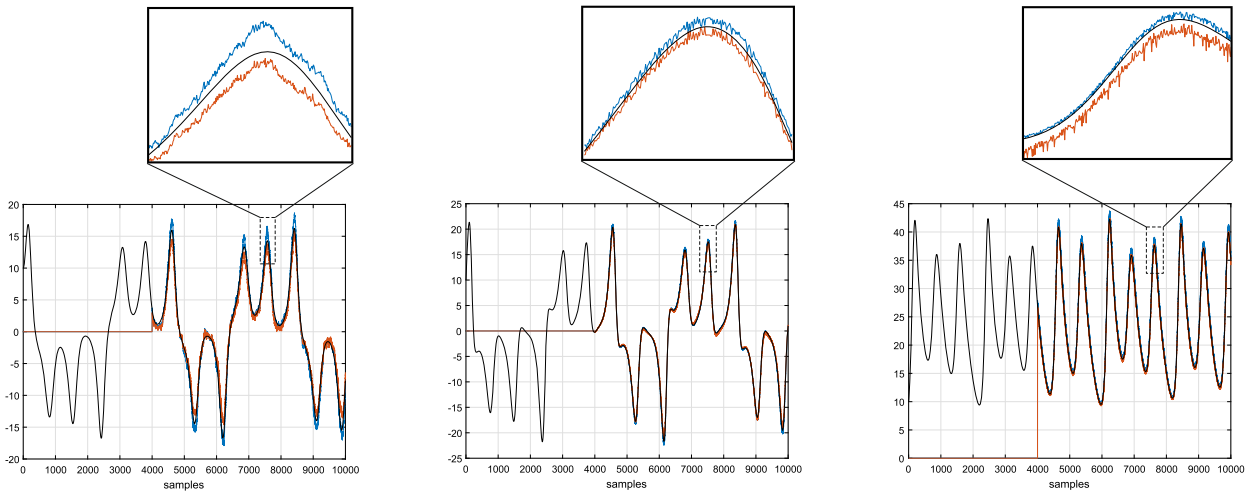


**(a)** The confidence region created by interval type-2 fuzzy Kalman filter for filtering and tracking the state variable $x_1$ of Lorenz chaotic attractor.

**(b)** The confidence region created by interval type-2 fuzzy Kalman filter for filtering and tracking the state variable $x_2$ of Lorenz chaotic attractor.

**(c)** The confidence region created by interval type-2 fuzzy Kalman filter for filtering and tracking the state variable $x_3$ of Lorenz's chaotic attractor.

**Fig. 8** Performance of interval type-2 fuzzy Kalman filter, based on proposed methodology, for filtering and tracking the state variables $x_1$, $x_2$ and $x_3$ of Lorenz's chaotic attractor, in the case of $SNR = 0.65$

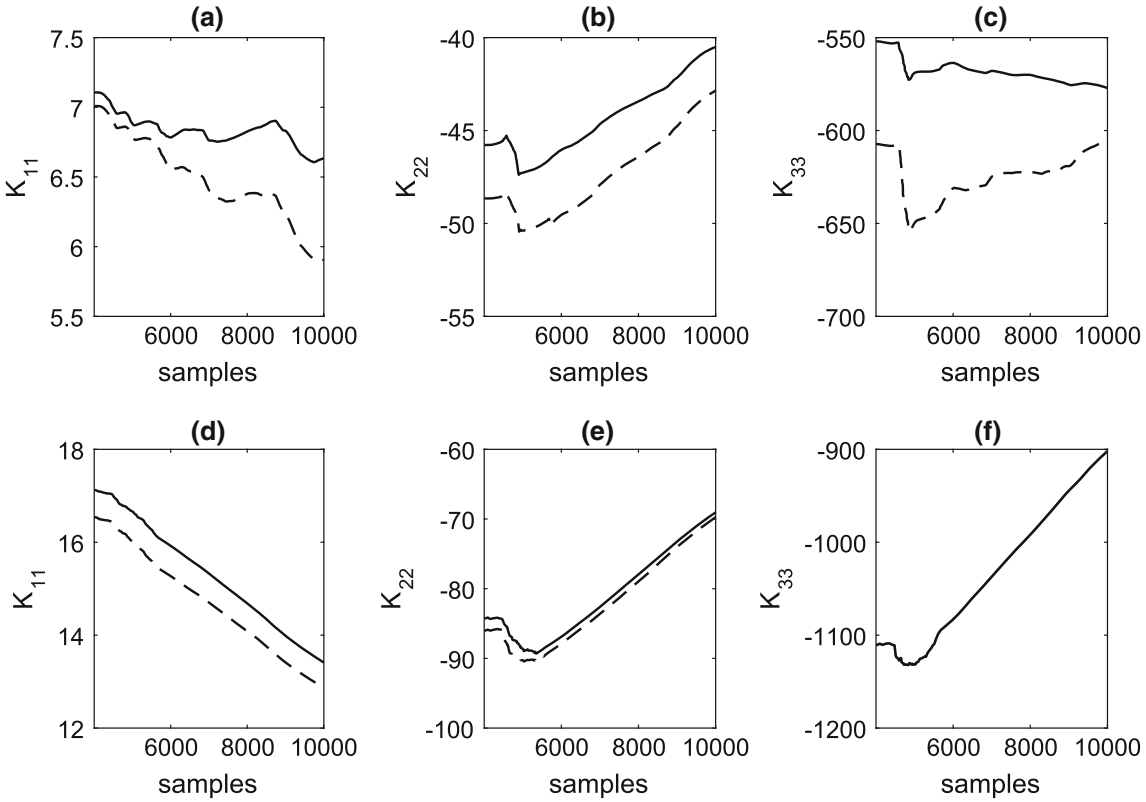


**Fig. 9** The temporal behavior estimated of the main diagonal elements from interval type-2 fuzzy Kalman gains, during recursive updating of interval type-2 fuzzy Kalman filter for filtering and tracking the state variables $x_1$, $x_2$ and $x_3$ of Lorenz's chaotic attractor: **a**–**c** Rule 1, **d**–**f** Rule 2

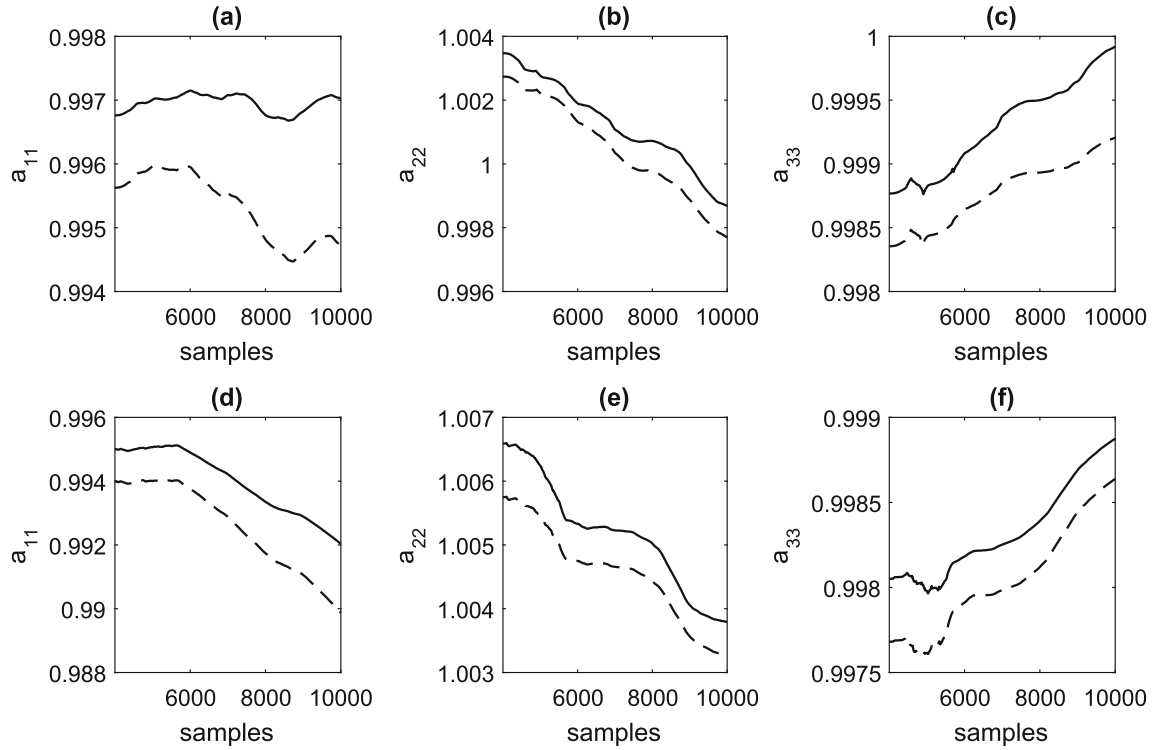


**Fig. 10** The temporal behavior from estimated of the main diagonal elements from interval type-2 fuzzy matrix $\widetilde{\mathbf{A}}^i$, during recursive updating of interval type-2 fuzzy Kalman filter for filtering and tracking the state variables $x_1$, $x_2$ and $x_3$ of Lorenz's chaotic attractor: **a**–**c** Rule 1, **d**–**f** Rule 2

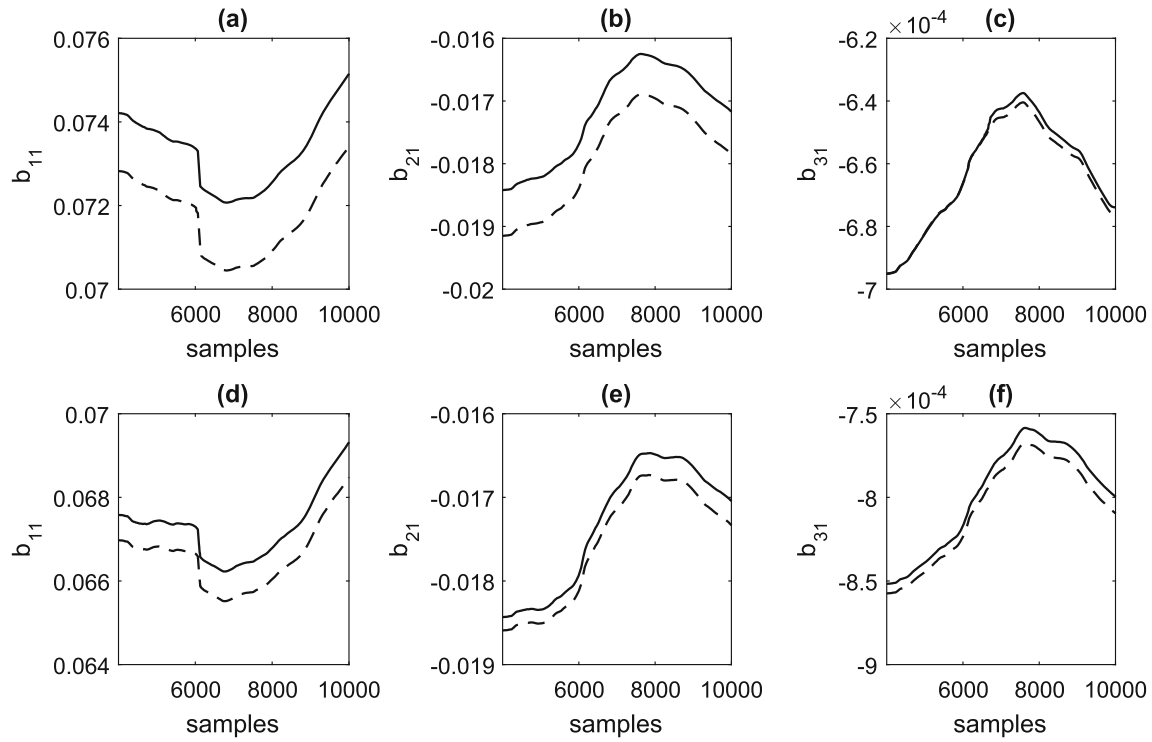


**Fig. 11** The temporal behavior from estimated of the main diagonal elements from interval type-2 fuzzy matrix $\widetilde{\mathbf{B}}^i$, during recursive updating of interval type-2 fuzzy Kalman filter for filtering and tracking the state variables $x_1$, $x_2$ and $x_3$ of Lorenz's chaotic attractor: **a**–**c** Rule 1, **d**–**f** Rule 2

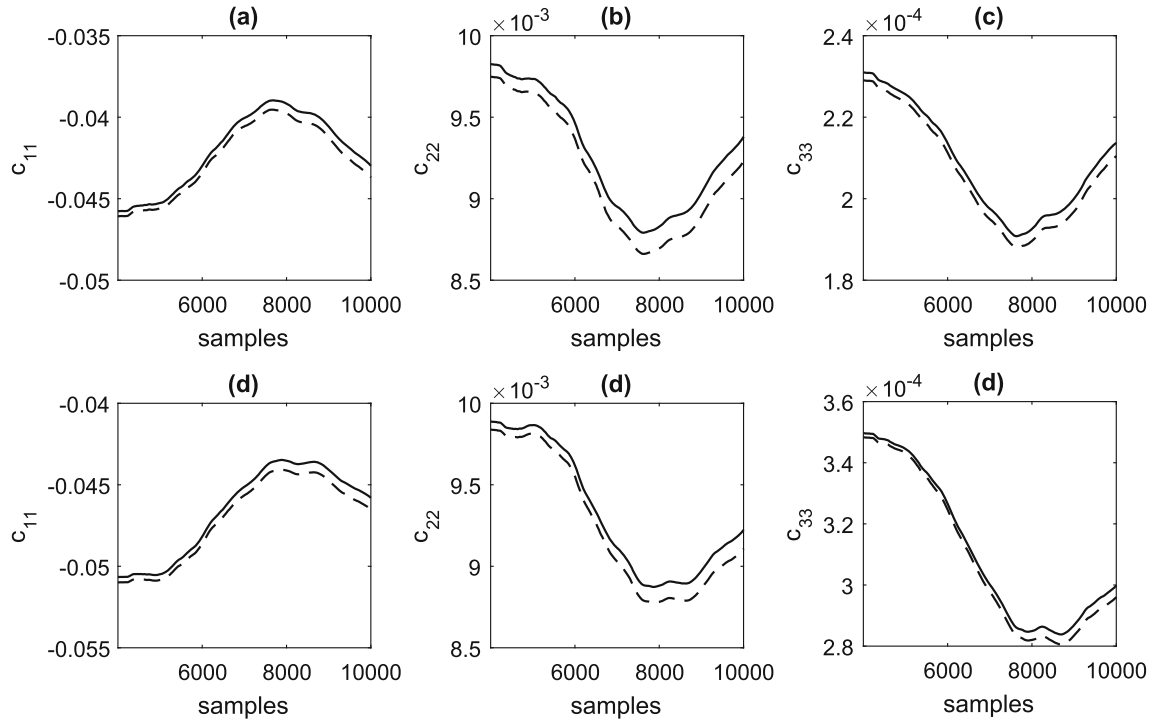


**Fig. 12** The temporal behavior from estimated of the main diagonal elements from interval type-2 fuzzy matrix $\widetilde{\mathbf{C}}^i$, during recursive updating of interval type-2 fuzzy Kalman filter for filtering and tracking the state variables $x_1$, $x_2$ and $x_3$ of Lorenz's chaotic attractor: **a**–**c** Rule 1, **d**–**f** Rule 2

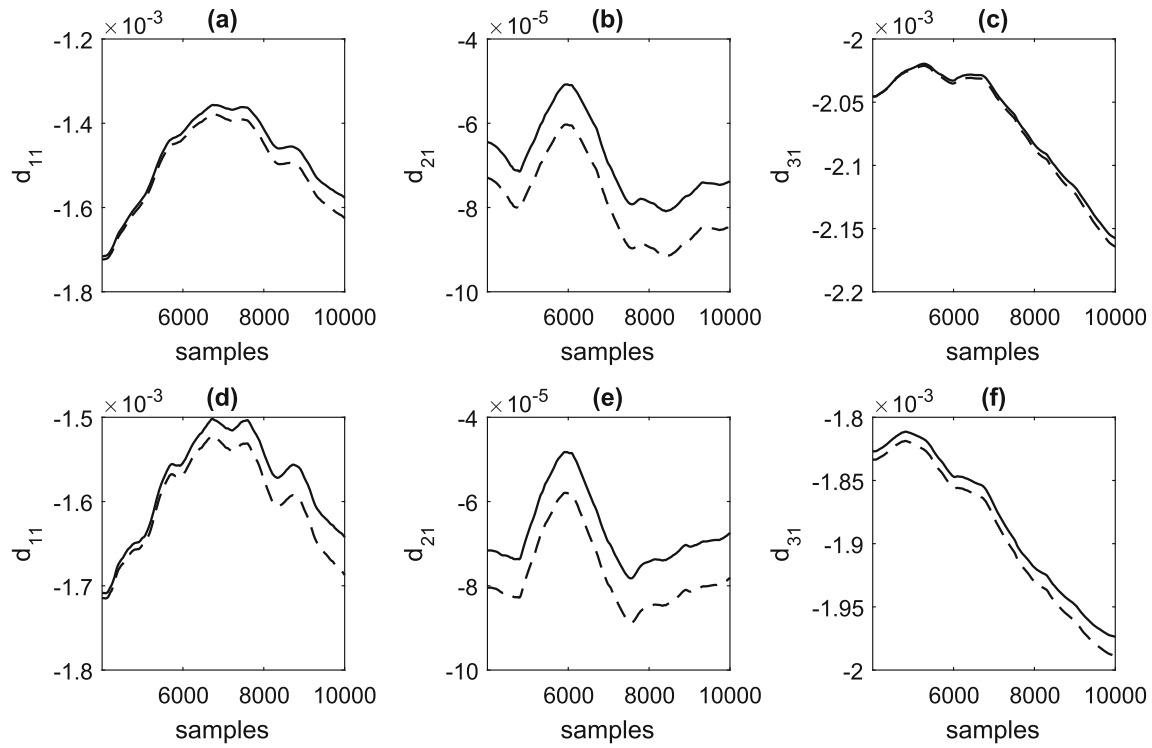


**Fig. 13** The temporal behavior from estimated of the main diagonal elements from interval type-2 fuzzy matrix $\widetilde{\mathbf{D}}^i$, during recursive updating of interval type-2 fuzzy Kalman filter for filtering and tracking the state variables $x_1$, $x_2$ and $x_3$ of Lorenz's chaotic attractor: **a**–**c** Rule 1, **d**–**f** Rule 2

and the observer gain Markov parameters are obtained by:

$$\widetilde{\mathbf{Y}}_1^{i^o} = \widetilde{\overline{\mathbf{Y}}}_1^{i^{(2)}} = \widetilde{\mathbf{C}}_k^i \widetilde{\mathbf{K}}_k^i \tag{41}$$

$$\widetilde{\mathbf{Y}}_j^{i^o} = \widetilde{\overline{\mathbf{Y}}}_j^{i^{(2)}} - \sum_{\iota=1}^{j-1} \widetilde{\overline{\mathbf{Y}}}_j^{i^{(2)}} \widetilde{\mathbf{Y}}_{j-\iota}^{i^o}, \text{ for } j = 2, \ldots, q \tag{42}$$

$$\widetilde{\mathbf{Y}}_j^{i^o} = -\sum_{\iota=1}^{q} \widetilde{\overline{\mathbf{Y}}}_j^{i^{(2)}} \widetilde{\mathbf{Y}}_{j-\iota}^{i^o}, \quad \text{for } j = q+1, \ldots, \infty \tag{43}$$

**Step 4** - Construct the Hankel matrix $\widetilde{\mathbf{H}}^i\ (j-1) \in \mathbb{R}^{\gamma p \times \beta m}$:

$$\widetilde{\mathbf{H}}^i\ (j-1) = \begin{bmatrix} \widetilde{\mathbf{Y}}_j^i & \widetilde{\mathbf{Y}}_{j+1}^i & \cdots & \widetilde{\mathbf{Y}}_{j+\beta-1}^i \\ \widetilde{\mathbf{Y}}_{j+1}^i & \widetilde{\mathbf{Y}}_{j+2}^i & \cdots & \widetilde{\mathbf{Y}}_{j+\beta}^i \\ \vdots & \vdots & \ddots & \vdots \\ \widetilde{\mathbf{Y}}_{j+\gamma-1}^i & \widetilde{\mathbf{Y}}_{j+\gamma}^i & \cdots & \widetilde{\mathbf{Y}}_{j+\gamma+\beta-2}^i \end{bmatrix} \tag{44}$$

where $\gamma$ and $\beta$ are sufficiently large arbitrary integers defined by user.

**Step 5** - For $j = 1$, decompose $\widetilde{\mathbf{H}}^i\ (0)$ using Singular Value Decomposition:

$$\widetilde{\mathbf{H}}^i\ (0) = \widetilde{\mathbf{\Xi}}^i \widetilde{\mathbf{\Sigma}}^i \widetilde{\mathbf{\Psi}}^{i^T} \tag{45}$$

where $\widetilde{\mathbf{\Xi}}^i \in \mathbb{R}^{\alpha p \times \alpha p}$ and $\widetilde{\mathbf{\Psi}}^i \in \mathbb{R}^{\beta m \times \beta m}$ are orthogonal matrices and $\widetilde{\mathbf{\Sigma}}^i \in \mathbb{R}^{\alpha p \times \beta m}$ is the diagonal matrix of singular values defined as:

$$\widetilde{\mathbf{\Sigma}}^i = \begin{bmatrix} \widetilde{\mathbf{\Sigma}}_n^i & 0 \\ 0 & 0 \end{bmatrix} \tag{46}$$

such that $n$ is the number of significant singular values and determines the minimum order of the type-2 fuzzy Kalman filter. Thus, the size of matrices in Eq. (45) is reduced to the minimum order, as follows:

$$\widetilde{\mathbf{H}}_n^i\ (0) = \widetilde{\mathbf{\Xi}}_n^i \widetilde{\mathbf{\Sigma}}_n^i \widetilde{\mathbf{\Psi}}_n^{i^T} \tag{47}$$

where $\widetilde{\mathbf{\Xi}}_n^i \in \mathbb{R}^{\alpha p \times n}$, $\widetilde{\mathbf{\Psi}}_n^i \in \mathbb{R}^{\beta m \times n}$, $\widetilde{\mathbf{\Sigma}}_n^i \in \mathbb{R}^{n \times n}$ are the resulting matrices after the reduction to minimum order.

**Step 6** - Compute the observability and controllability matrices:

$$\widetilde{\mathcal{P}}_\gamma^i = \widetilde{\mathbf{\Xi}}_n^i \left(\widetilde{\mathbf{\Sigma}}_n^i\right)^{1/2} \tag{48}$$

$$\widetilde{\mathcal{Q}}_\beta^i = \left(\widetilde{\mathbf{\Sigma}}_n^i\right)^{1/2} \widetilde{\mathbf{\Psi}}_n^{i^T} \tag{49}$$

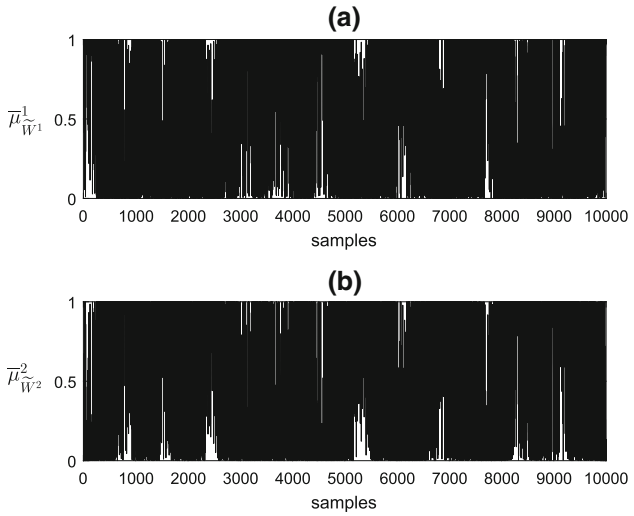


**Fig. 14** Instantaneous upper normalized fuzzy activation degrees of type-2 fuzzy Kalman inference system, during its recursive updating for filtering and tracking the state variables $x_1$, $x_2$ and $x_3$ of Lorenz's chaotic attractor: **a** Rule 1, **b** Rule 2

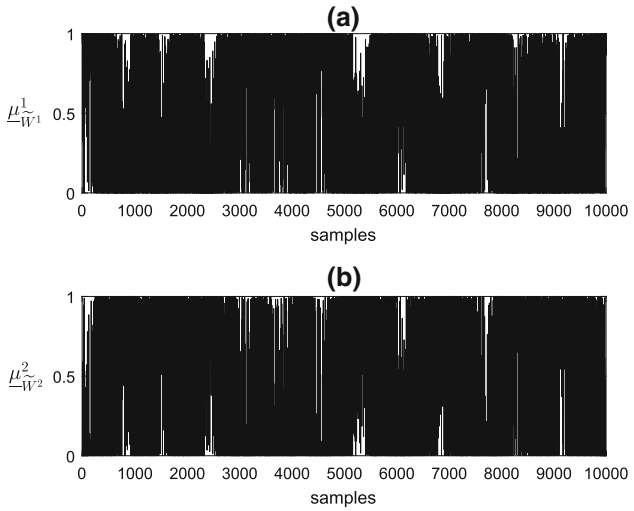


**Fig. 15** Instantaneous lower normalized fuzzy activation degrees of type-2 fuzzy Kalman inference system, during its recursive updating for filtering and tracking the state variables $x_1$, $x_2$ and $x_3$ of Lorenz's chaotic attractor: **a** Rule 1, **b** Rule 2

where

$$\widetilde{\mathcal{P}}_\gamma^i = \begin{bmatrix} \widetilde{\mathbf{C}}_k^i \\ \widetilde{\mathbf{C}}_k^i \widetilde{\mathbf{A}}_k^i \\ \widetilde{\mathbf{C}}_k^i \widetilde{\mathbf{A}}_k^{i^2} \\ \vdots \\ \widetilde{\mathbf{C}}_k^i \widetilde{\mathbf{A}}_k^{i^{\gamma-1}} \end{bmatrix} \tag{50}$$

is the observability matrix and

$$\widetilde{\mathcal{Q}}_\beta^i = \begin{bmatrix} \widetilde{\mathbf{B}}_k^i & \widetilde{\mathbf{A}}_k^i \widetilde{\mathbf{B}}_k^i & \widetilde{\mathbf{A}}_k^{i^2} \widetilde{\mathbf{B}}_k^i & \cdots & \widetilde{\mathbf{A}}_k^{i^{\beta-1}} \widetilde{\mathbf{B}}_k^i \end{bmatrix} \tag{51}$$

is the controllability matrix.

**Step 7** - Compute the matrices that make up the consequent proposition of interval type-2 fuzzy Kalman filter:

$$\widetilde{\mathbf{A}}_k^i = \left(\widetilde{\mathbf{\Sigma}}_n^i\right)^{-1/2} \widetilde{\mathbf{\Xi}}_n^{i^T} \widetilde{\mathbf{H}}_n^i \,(1)\, \widetilde{\mathbf{\Psi}}_n^{i^T} \left(\widetilde{\mathbf{\Sigma}}_n^i\right)^{-1/2} \tag{52}$$

$$\widetilde{\mathbf{B}}_k^i = \text{first } m \text{ columns of } \mathcal{Q}_\beta^i \tag{53}$$

$$\widetilde{\mathbf{C}}_k^i = \text{first } p \text{ rows of } \mathcal{P}_\beta^i \tag{54}$$

$$\widetilde{\mathbf{D}}_k^i = \widetilde{\mathbf{Y}}_0^i \tag{55}$$

**Step 8** - Compute the interval Kalman gain matrix:

$$\widetilde{\mathbf{Y}}_j^{i^o} = -\widetilde{\mathcal{P}}_\beta^i \widetilde{\mathbf{K}}_k^i \tag{56}$$

where $\widetilde{\mathbf{Y}}_j^{i^o}$ is the observer gain Markov parameters, $\widetilde{\mathcal{P}}_\beta^i$ is the observability matrix and $\widetilde{\mathbf{K}}_k^i$ is the interval Kalman gain matrix. Manipulating Eq. (56):

$$\widetilde{\mathcal{P}}_\beta^{i^T} \widetilde{\mathbf{\Gamma}}^i \widetilde{\mathbf{Y}}_j^{i^o} = -\widetilde{\mathcal{P}}_\beta^{i^T} \widetilde{\mathbf{\Gamma}}^i \widetilde{\mathcal{P}}_\beta^i \widetilde{\mathbf{K}}_k^i \tag{57}$$

Assuming $\widetilde{\mathfrak{A}}^i = -\widetilde{\mathcal{P}}_\beta^{i^T} \widetilde{\mathbf{\Gamma}}^i \widetilde{\mathcal{P}}_\beta^i$ and $\widetilde{\mathfrak{N}}^i = \widetilde{\mathcal{P}}_\beta^{i^T} \widetilde{\mathbf{\Gamma}}^i \widetilde{\mathbf{Y}}_j^{i^o}$, Eq. (57) is rewritten as follows:

$$\widetilde{\mathfrak{A}}^i \widetilde{\mathbf{K}}_k^i = \widetilde{\mathfrak{N}}^i \tag{58}$$

Equation (58) is solved by QR factorization method being applied to $\widetilde{\mathfrak{A}}^i$ and obtaining the interval Kalman gain matrix $\widetilde{\mathbf{K}}_k^i$ in the same way as done in **Step 2** for determining interval Markov parameters.

*Recursive Updating of Interval Type-2 Fuzzy Kalman Filter Inference System* After the initial estimation of interval type-2 fuzzy Kalman filter, the Kalman filters, into consequent proposition of interval type-2 fuzzy Kalman filter inference system, are updated recursively at instants of time $k = N_b + 1, k = N_b + 2, \ldots$, to each new sample from experimental data set. Considering the regressors vector, at instant $k$, given by

$$\boldsymbol{\lambda}_k = \begin{bmatrix} \mathbf{u}_{k+1} \\ \mathbf{Z}_k \\ \mathbf{Z}_{k-1} \\ \vdots \\ \mathbf{Z}_{k-q} \end{bmatrix} \tag{59}$$

the interval observer Markov parameters $\widetilde{\widetilde{\mathbf{Y}}}^i$ are obtained by recursive updating of Eq. (32), as follows:

$$\widetilde{\mathfrak{U}}_k^i = \widetilde{\mathfrak{U}}_{k-1}^i + \widetilde{\mu}_{\widetilde{W}^i}^i(\mathbf{Z}_k)\boldsymbol{\lambda}_k\boldsymbol{\lambda}_k^T \tag{60}$$

$$\widetilde{\mathfrak{K}}_k^i = \widetilde{\mathfrak{K}}_{k-1}^i + \widetilde{\mu}_{\widetilde{W}^i}^i(\mathbf{Z}_k)\boldsymbol{\lambda}_k\mathbf{y}_k^T \tag{61}$$

Once $\widetilde{\mathfrak{U}}_k^i$ and $\widetilde{\mathfrak{K}}_k^i$ have been updated, and applying the QR factorization in $\widetilde{\mathfrak{U}}_k^i$, the $i$-th Markov parameters are updated. The consequent proposition of the type-2 fuzzy Kalman filter is updated recursively by repeating the Step 3 to Step 7. Similarly, the interval type-2 fuzzy Kalman gain matrix $\widetilde{\mathbf{K}}_k^i$ is obtained by recursive updating of Eq. (58), as follows:

$$\widetilde{\mathfrak{A}}_k^i = \widetilde{\mathfrak{A}}_{k-1}^i + \widetilde{\mu}_{\widetilde{W}^i}^i(\mathbf{Z}_k)\boldsymbol{\lambda}_k\boldsymbol{\lambda}_k^T \tag{62}$$

$$\widetilde{\mathfrak{N}}_k^i = \widetilde{\mathfrak{N}}_{k-1}^i + \widetilde{\mu}_{\widetilde{W}^i}^i(\mathbf{Z}_k)\boldsymbol{\lambda}_k\boldsymbol{\lambda}_k^T \tag{63}$$

Once $\widetilde{\mathfrak{A}}_k^i$ and $\widetilde{\mathfrak{N}}_k^i$ have been updated, and applying the QR factorization method in $\widetilde{\mathfrak{A}}_k^i$, the interval type-2 fuzzy Kalman gain matrix is updated.

The interval type-2 fuzzy Observer/Kalman Filter Identification algorithm, according to proposed methodology, is implemented as described in Algorithm 4.

## 3 Results

In this section, computational results from filtering and tracking the states of a nonlinear dynamic system with chaotic behavior in a noisy environment, are shown to illustrate the efficiency of proposed methodology in comparison to approach in (Páramo-Carranza et al. 2017). Also, experimental results from real-time interval tracking and forecasting the COVID-19's dynamic spread behavior in state of Maranhão and Brazil are shown to demonstrate the applicability of proposed methodology.

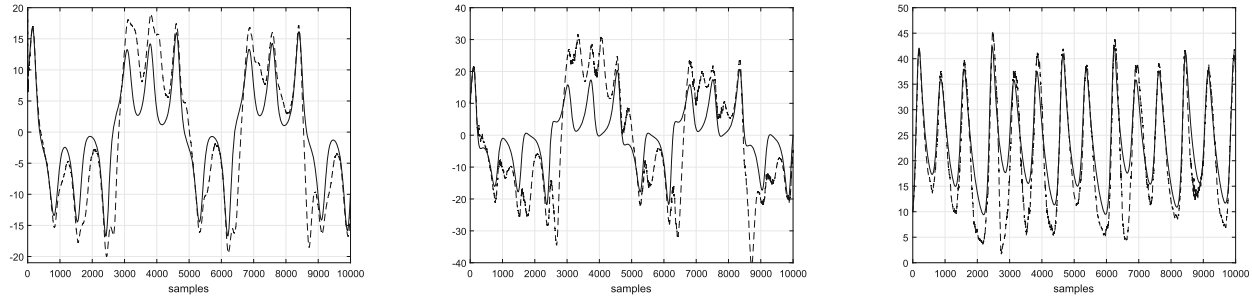


**(a)** The temporal behavior for filtering and tracking the state variable $x_1$ of Lorenz's chaotic attractor.

**(b)** The temporal behavior for filtering and tracking the state variable $x_2$ of Lorenz's chaotic attractor.

**(c)** The temporal behavior for filtering and tracking the state variable $x_3$ of Lorenz's chaotic attractor.

**Fig. 16** Performance of approach in (Páramo-Carranza et al. 2017) (dashed line) for filtering and tracking the state variables $x_1$, $x_2$ and $x_3$ of Lorenz's chaotic attractor (solid line), in the case of $SNR = 0.65$

**Table 1** Efficiency analysis of interval type-2 fuzzy Kalman filter, based on proposed methodology, as compared to approach in (Páramo-Carranza et al. 2017), for filtering and tracking the state variables $x_1$, $x_2$ and $x_3$ of Lorenz's chaotic attractor in the case of $SNR = 0.65$, based on MSE validation criterion

| | $\text{MSE}_{x_1}$ | $\text{MSE}_{x_2}$ | $\text{MSE}_{x_3}$ |
|---|---|---|---|
| Approach in (Páramo-Carranza et al. 2017) | 33.7164 | 173.6338 | 23.6985 |
| upper limit of interval type-2 fuzzy Kalman filter (proposed methodology) | 1.6826 | 0.0145 | 0.1033 |
| lower limit of interval type-2 fuzzy Kalman filter (proposed methodology) | 2.1672 | 0.1255 | 0.1571 |

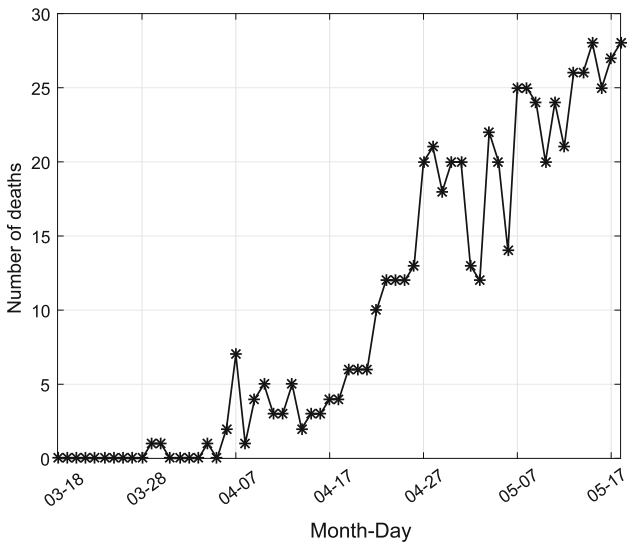


**Fig. 17** The experimental data of daily deaths reports within period ranging from 18 of March 2020 to 18 of May 2020, in state of Maranhão

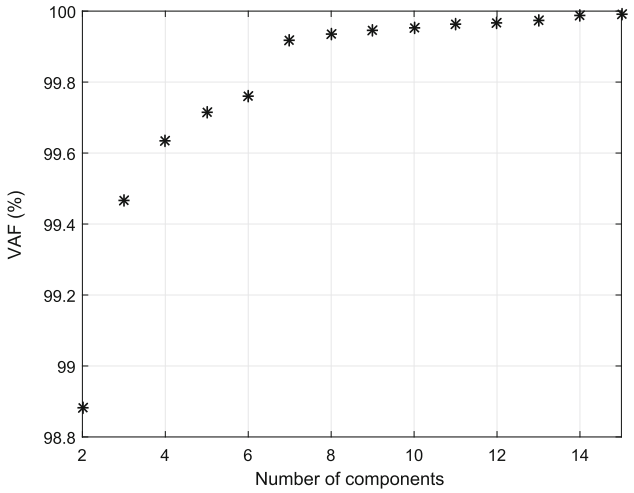


**Fig. 18** The efficiency of unobservable components, according to VAF criterion, for representing the experimental data of the daily deaths reports, in the state of Maranhão

## 3.1 Computational Results

### 3.1.1 Interval Type-2 Fuzzy Kalman Filtering and Tracking of Lorenz's Chaotic Attractor

In this section, computational results for filtering and tracking the states of a nonlinear dynamic system, with chaotic behavior, in a noisy environment, for comparative analysis with the approach in (Páramo-Carranza et al. 2017), widely cited in the literature, are presented. The nonlinear dynamic system under analysis consists of the Lorenz's chaotic attrac-

**Algorithm 4:** Interval Type-2 Fuzzy Observer/Kalman Filter Identification Algorithm

**input** : $\mathbf{Z}, \gamma, \beta, q, \widetilde{\mathbf{\Gamma}}^i$

**output**: $\widetilde{\mathbf{A}}_k^i, \widetilde{\mathbf{B}}_k^i, \widetilde{\mathbf{C}}_k^i, \widetilde{\mathbf{D}}_k^i, \widetilde{\mathbf{K}}_k^i$

Construct the matrix of regressors $\mathbf{\Lambda}$ - Eq. (25);

*%Training step*;

**for** $i = 1$ **to** $c$ **do**

**Step 1**: Compute the interval observer Markov parameters $\widetilde{\overline{\mathbf{Y}}}^i$ - Eq. (31)-(33);

**Step 2**: Compute the interval system Markov parameters $\widetilde{\mathbf{Y}}^i$ - Eq. (38)-(40);

**Step 3**: Compute the interval observer gain Markov parameters $\widetilde{\mathbf{Y}}^{i^o}$ - Eq. (41)-(43);

**Step 4**: Construct the Hankel matrices $\widetilde{\mathbf{H}}^i$ (0) and $\widetilde{\mathbf{H}}^i$ (1) - Eq. (44);

**Step 5**: Decompose $\widetilde{\mathbf{H}}^i$ (0) using SVD method - Eq. (45) and determine the minimum order of realization $n$ for the application - Eq. (46);

**Step 6**: Compute the observability matrix $\widetilde{\boldsymbol{\mathcal{P}}}_\gamma^i$ - Eq. (48) and the controllability matrix $\widetilde{\boldsymbol{\mathcal{Q}}}_\beta^i$ - Eq. (49);

**Step 7**: Compute the matrices $\widetilde{\mathbf{A}}_k^i, \widetilde{\mathbf{B}}_k^i, \widetilde{\mathbf{C}}_k^i, \widetilde{\mathbf{D}}_k^i$ - Eq. (52)-(55);

**Step 8**: Compute the interval Kalman gain matrix $\widetilde{\mathbf{K}}_k^i$ - Eq. (56)-(58);

**end**

*%Recursive update of interval type-2 fuzzy Kalman filter*;

**while** $k \geq N_b + 1$ **do**

**Step 1**: Construct the regressors vector $\boldsymbol{\lambda}_k$ - Eq. (59);

**for** $i = 1$ **to** $c$ **do**

**Step 2**: Update the interval Markov parameters through Eq. (60)-(61);

**Step 3**: Repeat **Step 3** to **Step 7** described in training step;

**Step 4**: Update the interval Kalman gain matrix through Eq. (62)-(63)

**end**

**end**

tor, described by (Huang et al. 2015):

$$\begin{aligned}\dot{x}_1 &= \varrho(x_2 - x_1)\\ \dot{x}_2 &= \varpi x_1 - x_2 - x_1 x_3\\ \dot{x}_3 &= x_1 x_2 - \varkappa x_3\end{aligned} \tag{64}$$

where the parameters $\varrho = 10$, $\varkappa = 8/3$ and $\varpi = 28$ provide a chaotic behavior.

Once that the problem of interest, in this paper, is based on the time series related to state variables $x_1$, $x_2$ and $x_3$ from Lorenz's chaotic attractor, the variable $\mathbf{u}_k$, in Eq. 15 of proposed methodology, is considered as white noise signal with low amplitude. A data set from Lorenz's chaotic attractor, with total length of 10000 samples by a sampling period of $T = 1$ ms, was generated. The first 4000 samples were used in training step for initial parameterization of interval type-2 fuzzy Kalman filter. The unobservable components associated to state variable $x_1$ of Lorenz's chaotic attractor were extracted by singular spectral analysis approach, according to section 2.1, for pre-processing of data set. The noisy state variable $x_1$ was decomposed into 2 spectral components, where the component with residual behavior was used for estimation of measurement noise covariance $R_k$ and weighting factor $\boldsymbol{\mathcal{X}}$, and the other component, assuming correlated to nominal dynamic of state variable $x_1$, was used for parameterizing the interval type-2 fuzzy Kalman filter. The partitions of computational data from noisy state variable $x_1$ were defined by interval type-2 fuzzy Gustafson–Kessel clustering algorithm, so the antecedent proposition, the rules number and consequent proposition, of the interval type-2 fuzzy Kalman filter, could be estimated successfully. For implementing the interval type-2 fuzzy clustering algorithm, the following parameters were adopted: number of clusters $c = 2$, interval weighting exponent $\widetilde{m} = [1.5, 2.0]$ and termination tolerance $\mathcal{E} = 10^{-5}$. According to computational data of Lorenz's chaotic attractor state variables $x_2$ and $x_3$, the unobservable components from noisy state variable $x_1$, the interval type-2 fuzzy normalized membership values and the parameterization of interval type-2 fuzzy Kalman filter by training and recursive steps were performed. The parametric estimation of consequent proposition of interval type-2 fuzzy Kalman filter inference system, in Eq. 15, took into account the partitions on noisy state variable $x_1$ as weighting criterion, and the parameters values: $q = 1$, $\gamma = 10$ e $\beta = 10$. The signal-to-noise ratio (SNR) in the state variable $x_1$ was varied, so that the ultimate goal was for filtering and tracking, from noisy computational data set, the nominal state variables $x_1$, $x_2$ and $x_3$ as accurate as possible. The mean square error (MSE) values, used as validation criterion, for different levels of SNR, considering the effect of 100 realizations in the filtering and tracking the nominal state variables $x_1$, $x_2$ and $x_3$, are shown in Figs. 1, 2, 3, respectively. It is observed the superior performance of interval type-2 fuzzy Kalman filter, based on proposed methodology, for filtering and tracking the Lorenz's chaotic attractor state variables, considering the lower values of MSE obtained by upper and lower limits of the interval type-2 fuzzy Kalman filter as compared to values of MSE obtained by approach in (Páramo-Carranza et al. 2017).

Considering the particular case of $SNR = 0.65$, the dynamic behavior for noisy and nominal cases of Lorenz's chaotic attractor state variable $x_1$ is shown in Fig. 4. According to experimental data of state variable $x_1$ shown in Fig. 4, the pre-processed unobservable components in Fig. 5 and the interval type-2 fuzzy normalized membership values in Fig. 6, the parametric estimation of the type-2 fuzzy Kalman filter was computed by training and recursive steps. The com-

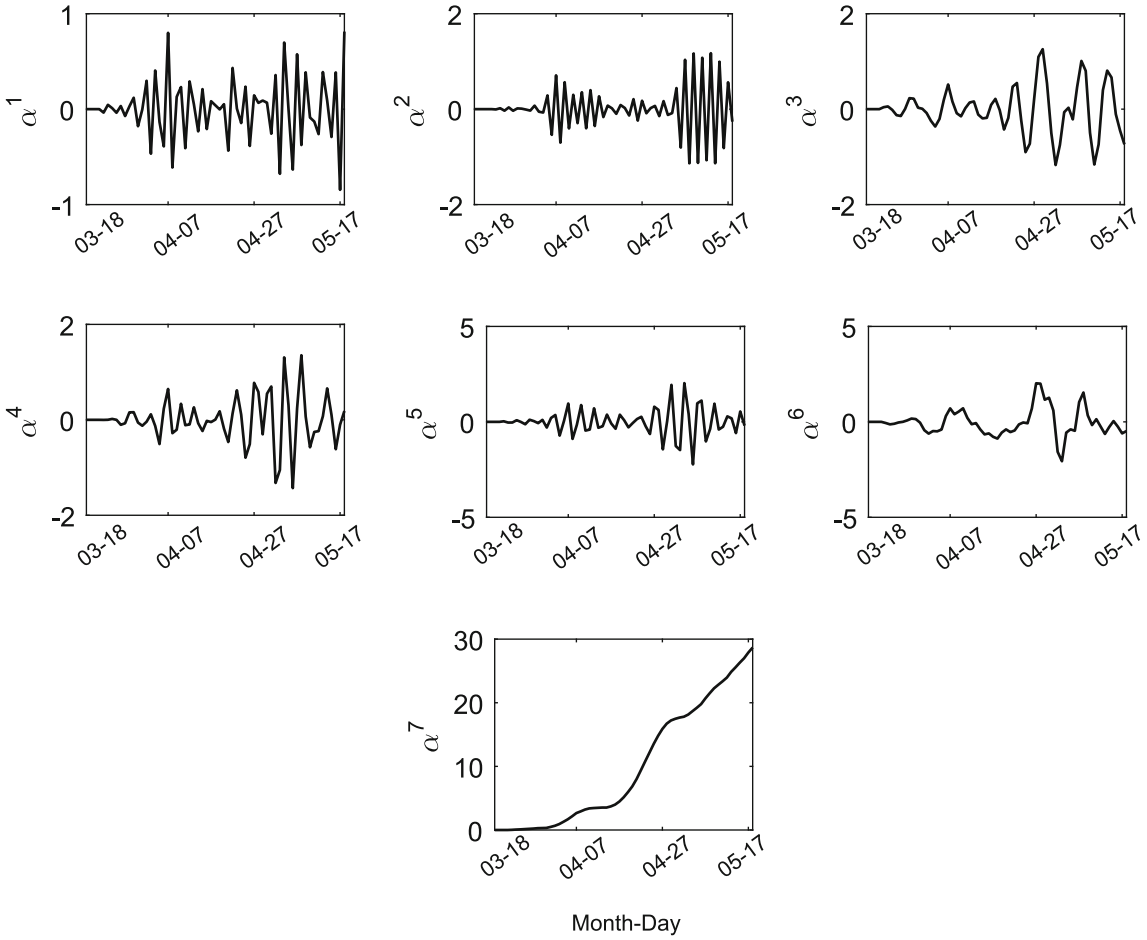


**Fig. 19** The temporal behavior of spectral unobservable components $\alpha^j|^{j=1,\ldots,7}$, which were extracted from experimental data of daily deaths, in the state of Maranhão

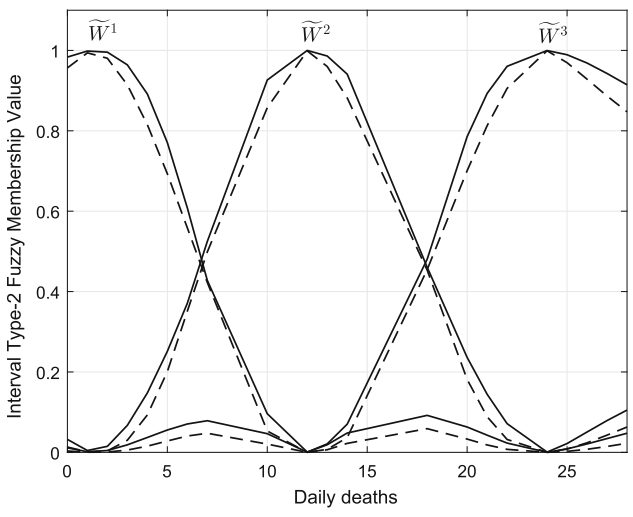


**Fig. 20** Interval type-2 fuzzy membership functions estimated from clustering of daily deaths reports, in state of Maranhão

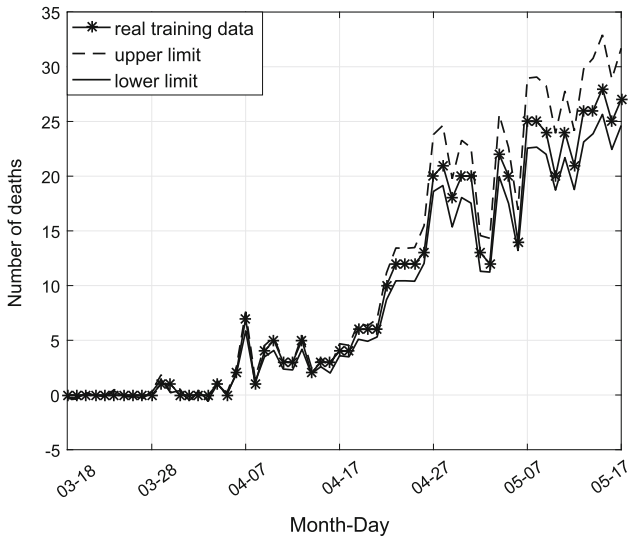


**Fig. 21** The confidence region generated by interval type-2 fuzzy Kalman filter for tracking the experimental data of daily deaths reports, from 03 of March 2020 to 18 of May 2020, in state of Maranhão

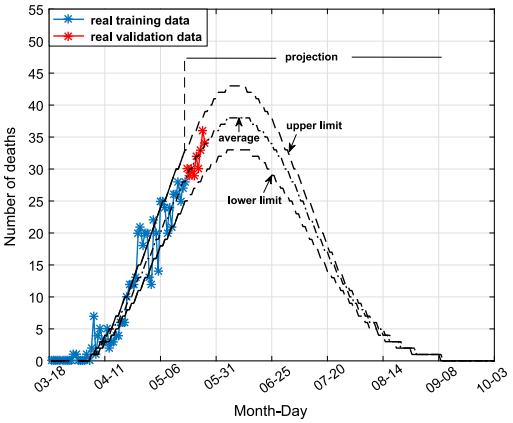


**(a)** The performance of interval type-2 fuzzy Kalman filter based on its initial estimation by training step for forecasting the future (validation) daily deaths reports within period ranging from 19 of May 2020 to 27 of May 2020, in state of Maranhão.

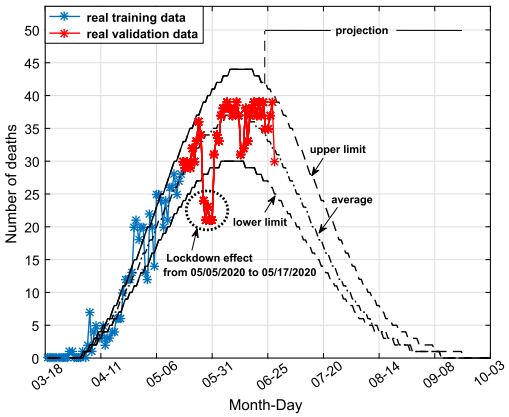


**(b)** The performance of interval type-2 fuzzy Kalman filter based on its recursive updating on 24 of June 2020 for forecasting the future (validation) daily deaths reports within the period ranging from 25 of June 2020 to 03 of July 2020, in state of Maranhão.

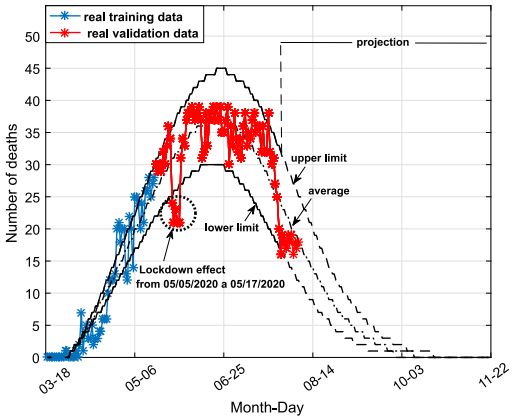


**(c)** The performance of interval type-2 fuzzy Kalman filter based on its recursive updating on 28 of July 2020 for forecasting the future (validation) daily deaths reports within the period ranging from 29 of July 2020 to 25 of August 2020, in state of Maranhão.

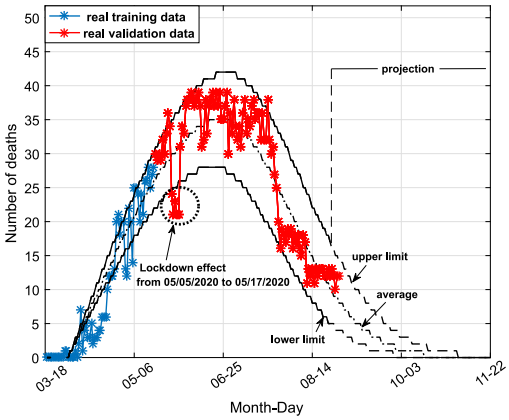


**(d)** The performance of interval type-2 fuzzy Kalman filter based on its recursive updating on 25 of August 2020 for forecasting the future (validation) daily deaths reports within the period ranging from 26 of August 2020 to 25 of September 2020, in state of Maranhão.

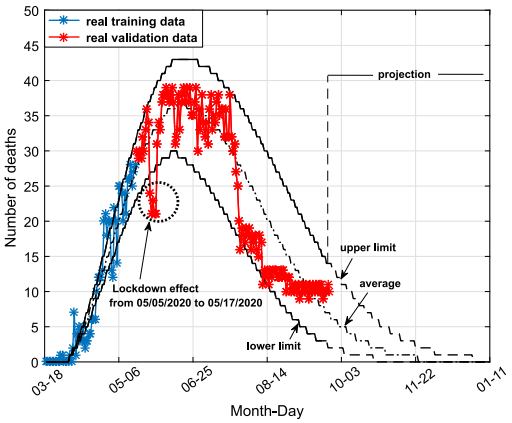


**(e)** The performance of interval type-2 fuzzy Kalman filter based on its recursive updating on 25 of September 2020 for forecasting the future (validation) daily deaths reports within the period ranging from 26 of September 2020 to ahead, in state of Maranhão.

**Fig. 22** Performance of the interval type-2 fuzzy Kalman filter for tracking and forecasting the effects of COVID-19 spread experimental data related to daily deaths reports, in state of Maranhão: **a** updating based on training data from 18 of March 2020 to 18 of May 2020; **b** recursive updating on 24 of June 2020; **c** recursive updating on 28 of July 2020; **d** recursive updating on 25 of August 2020; **e** recursive updating on 25 of September 2020

ponent with residual behavior was used for estimation of measurement noise covariance $R_k$ and weighting factor $\mathcal{X}$, and the other component, assuming correlated to nominal dynamic of state variable $x_1$, was used for parameterizing the interval type-2 fuzzy Kalman filter. As it can be seen in Fig. 5, the unobservable component $\alpha^1$ presenting a residual behavior was used for estimation of measurement noise covariance $R_k$ and weighting factor $\mathcal{X}$, and the unobservable component $\alpha^2$ assuming correlated to nominal dynamic of state variable $x_1$ was used for parameterizing the interval type-2 fuzzy Kalman filter. Based on estimation of measurement noise covariance $R_k$ associated to state variable $x_1$, the weighting factor $\mathcal{X}_k$ to be used as weighting factor for implementing the recursive updating mechanism of interval type-2 fuzzy Kalman filter is given by:

$$\mathcal{X}_k = \begin{bmatrix} R_k^{-1} & 0 & 0 \\ 0 & 1 & 0 \\ 0 & 0 & 1 \end{bmatrix} \tag{65}$$

The temporal behavior of the measurement noise covariance $R_k$ and the weighting factor $\mathcal{X}_k$, which are associated with filtering and tracking the state variable $x_1$ from Lorenz chaotic attractor, by interval type-2 fuzzy Kalman filter, is shown in Fig. 7. The confidence region, as shown in Fig. 8, created by interval type-2 fuzzy Kalman filter taking into account uncertainties, estimated by interval type-2 membership functions shown in Fig. 6, inherited to noisy data from Lorenz's chaotic attractor, illustrates its efficiency for filtering and tracking the state variables $x_1$, $x_2$ and $x_3$. The estimation of interval type-2 fuzzy Kalman gain matrices $\widetilde{\mathbf{K}}^i|^{i=1,\ldots,2}$, during recursive updating of interval type-2 fuzzy Kalman filter for filtering and tracking the state variables $x_1$, $x_2$ and $x_3$ of Lorenz's chaotic attractor, is shown in Fig. 9. The recursive estimation of the interval type-2 fuzzy matrices $\widetilde{\mathbf{A}}^i$, $\widetilde{\mathbf{B}}^i$, $\widetilde{\mathbf{C}}^i$ and $\widetilde{\mathbf{D}}^i$, with $i = 1, \ldots, 2$, in the consequent proposition of the interval type-2 fuzzy Kalman filter inference system, during recursive updating of interval type-2 fuzzy Kalman filter for filtering and tracking the state variables $x_1$, $x_2$ and $x_3$ of Lorenz's chaotic attractor, is shown in Figs. 10, 11, 12, 13. The upper and lower instantaneous activation degrees related to interval type-2 fuzzy Kalman filter inference system, for filtering and tracking the state variables $x_1$, $x_2$ and $x_3$ of Lorenz's chaotic attractor, are shown in Figs. 14, 15. The performance of approach in (Páramo-Carranza et al. 2017) for filtering and tracking the state variables $x_1$, $x_2$ and $x_3$ of the Lorenz's chaotic attractor is shown in Fig. 16.

The efficiency analysis of interval type-2 fuzzy Kalman filter by its comparison with approach in (Páramo-Carranza et al. 2017), for filtering and tracking the state variables $x_1$, $x_2$ and $x_3$ of Lorenz's chaotic attractor in the case of $SNR = 0.65$, based on MSE validation criterion, is shown in Tab. 1.

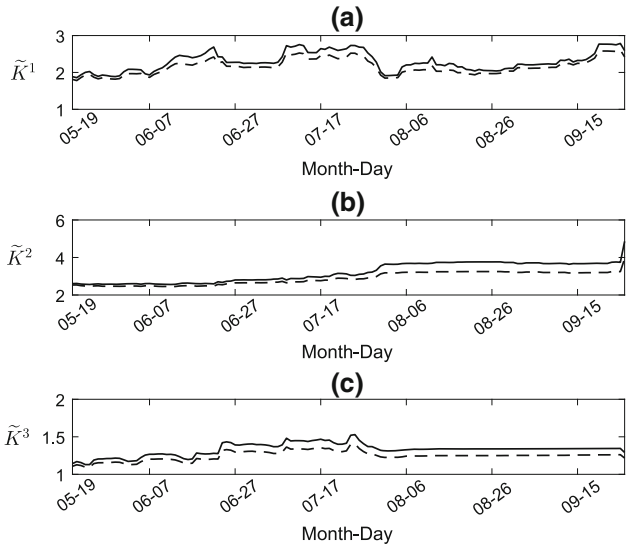


**Fig. 23** Interval type-2 fuzzy Kalman gains, during recursive updating of interval type-2 fuzzy Kalman filter for tracking and forecasting the COVID-19 dynamic spread experimental data related to daily deaths reports within period ranging from 19 of May 2020 to 25 of September, in state of Maranhão: **a** Rule 1, **b** Rule 2, **c** Rule 3

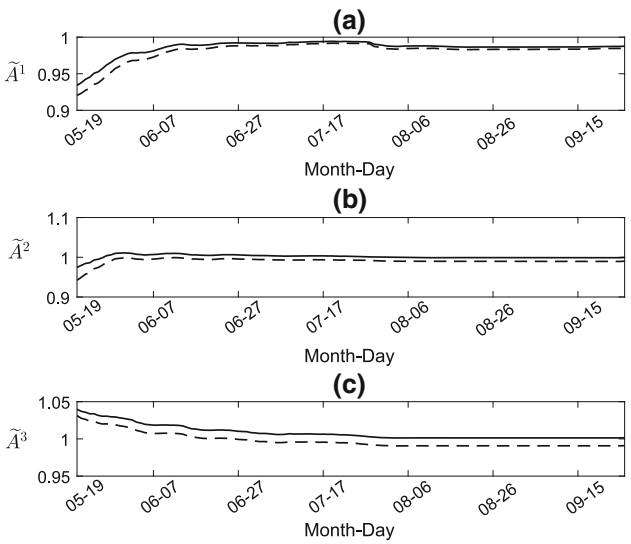


**Fig. 24** Interval type-2 fuzzy matrix $\widetilde{\mathbf{A}}^i$, during recursive updating of interval type-2 fuzzy Kalman filter for tracking and forecasting the COVID-19 dynamic spread experimental data related to daily deaths reports within period ranging from 19 of May 2020 to 25 of September, in state of Maranhão: **a** Rule 1, **b** Rule 2, **c** Rule 3

### 3.1.2 Comparative Analysis and Discussions

In this section, a more detailed discussion on the results shown in Figs. 1, 2, 3, 8, 16 and Table 1, according to comparative analysis of proposed methodology with the approach in (Páramo-Carranza et al. 2017), is presented.

The adopted methodology in (Páramo-Carranza et al. 2017) considers the fuzzy Kalman filter design procedure

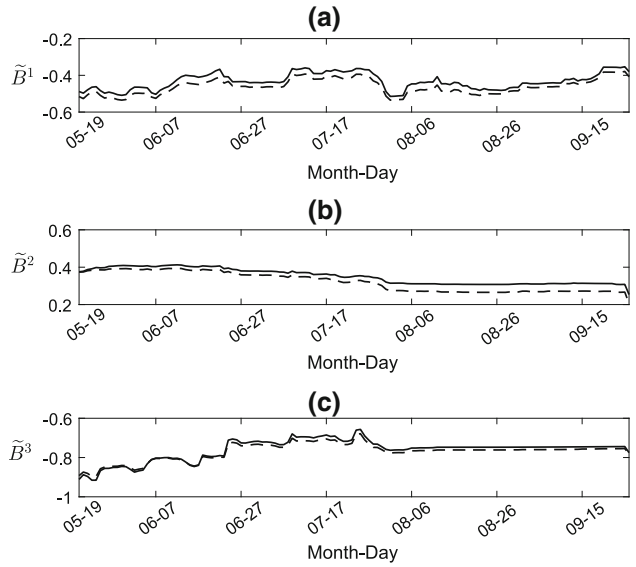


**Fig. 25** Interval type-2 fuzzy matrix $\widetilde{\mathbf{B}}^i$, during recursive updating of interval type-2 fuzzy Kalman filter for tracking and forecasting the COVID-19 dynamic spread experimental data related to daily deaths reports within period ranging from 19 of May 2020 to 25 of September, in state of Maranhão: **a** Rule 1, **b** Rule 2, **c** Rule 3

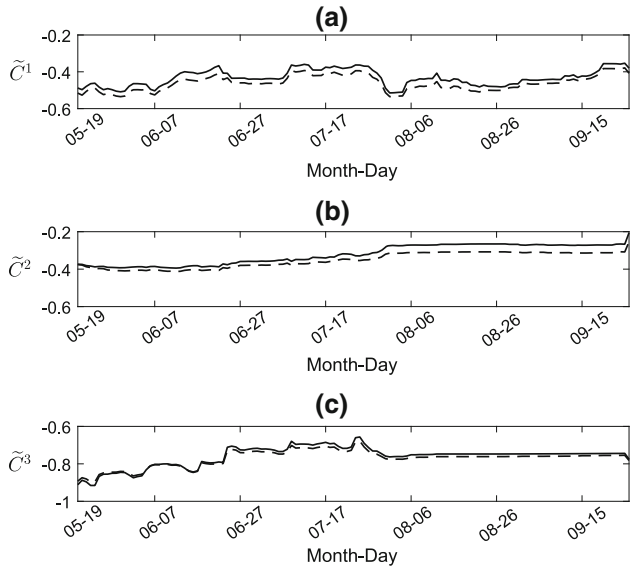


**Fig. 26** Interval type-2 fuzzy matrix $\widetilde{\mathbf{C}}^i$, during recursive updating of interval type-2 fuzzy Kalman filter for tracking and forecasting the COVID-19 dynamic spread experimental data related to daily deaths reports within period ranging from 19 of May 2020 to 25 of September, in state of Maranhão: **a** Rule 1, **b** Rule 2, **c** Rule 3

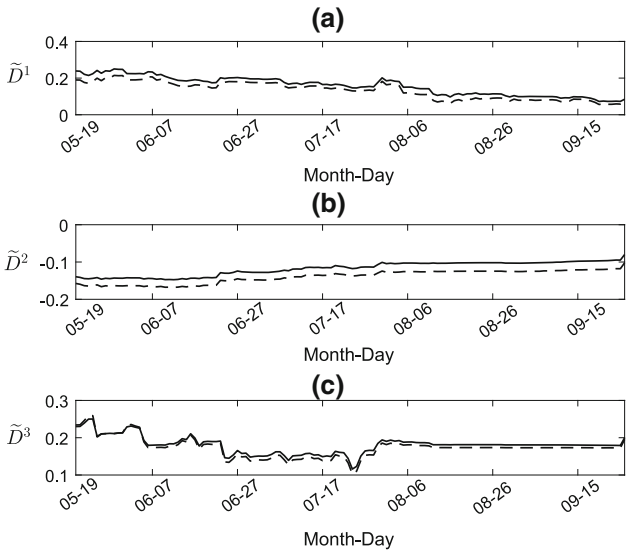


**Fig. 27** Interval type-2 fuzzy matrix $\widetilde{\mathbf{D}}^i$, during recursive updating of interval type-2 fuzzy Kalman filter for tracking and forecasting the COVID-19 dynamic spread experimental data related to daily deaths reports within period ranging from 19 of May 2020 to 25 of September, in state of Maranhão: **a** Rule 1, **b** Rule 2, **c** Rule 3

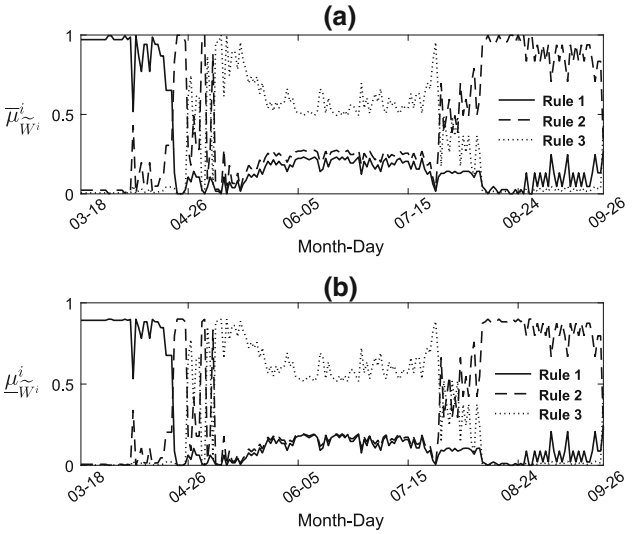


**Fig. 28** Instantaneous normalized fuzzy activation degrees of type-2 fuzzy Kalman inference system, during its recursive updating for tracking and forecasting the COVID-19 dynamic spread experimental data related to daily deaths reports within period ranging from 19 of May 2020 to 25 of September, in state of Maranhão: **a** upper instantaneous normalized fuzzy activation degrees and **b** lower instantaneous normalized fuzzy activation degrees

from discretization of the Lorenz chaotic nonlinear model in Eq. 64, the linearization at specific operation points of state variables $x_1$, $x_2$ and $x_3$, and the definition of membership functions with pre-established format for partitioning the dynamic behavior of states $x_1$, $x_2$ and $x_3$. The adopted discretization for fuzzy Kalman filter design is based on the current sample (at instant $k$) of the dynamic behavior of Lorenz chaotic attractor, discarding the previous information of samples, which implies a filter design based on dynamically limited discrete model and the filtering error accumulated at sample $k$ is propagated, recurrently, for further approximations, mainly in environments with high variability of experimental data, such as chaotic dynamic systems in a noisy environment, limiting the filtering per-

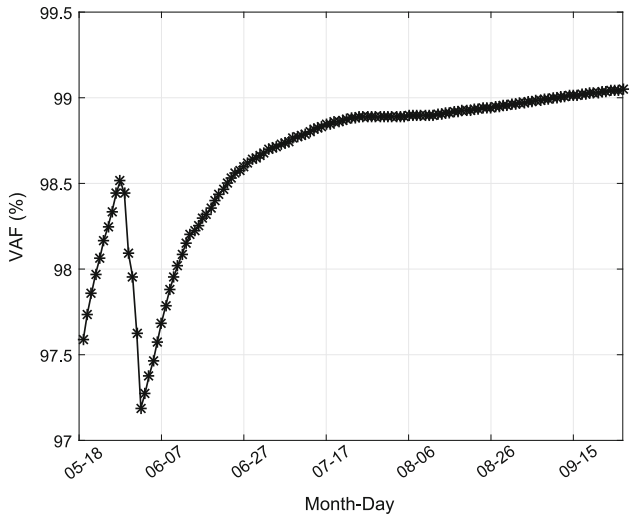


**Fig. 29** Real-time efficiency, based on VAF validation criterion, of interval type-2 fuzzy Kalman filter, during its recursive updating for tracking and forecasting the COVID-19 dynamic spread experimental data related to daily deaths reports within period ranging from 19 of May 2020 to 29 of September, in state of Maranhão

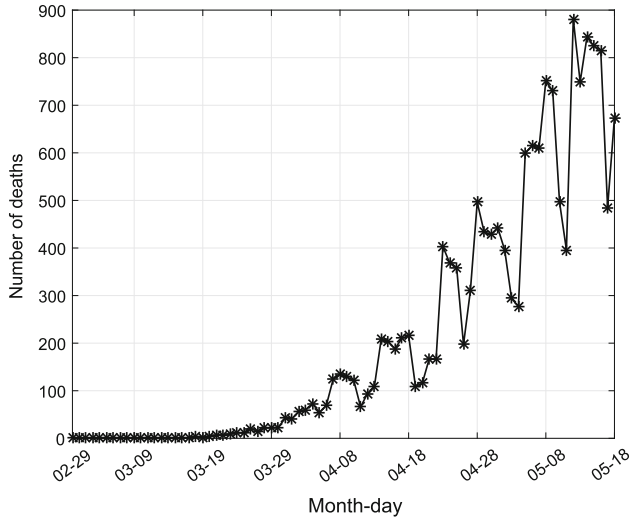


**Fig. 30** The experimental data of daily deaths reports within period from 29 of February 2020 to 18 of May 2020, in Brazil

formance for high errors (Franklin et al. 1997; Serra 2018). The adopted linearization considers the application of partial derivatives to Lorenz chaotic attractor in specific operation points of the state variables $x_1$, $x_2$ and $x_3$, which implies a filter design dynamically limited to specified operating points (Luenberger 1979; Chen 1999; Antsaklis and Liu 2003). Thus, as the dynamic behavior of Lorenz chaotic attractor, in a noisy environment, gets out the operating points of linearized state variables $x_1$, $x_2$ and $x_3$, the approximation errors increase in prediction and updating steps of discrete fuzzy Kalman filter and polarize the estimation of state variables $x_1$, $x_2$ and $x_3$. The adopted partitions of the discourse universe

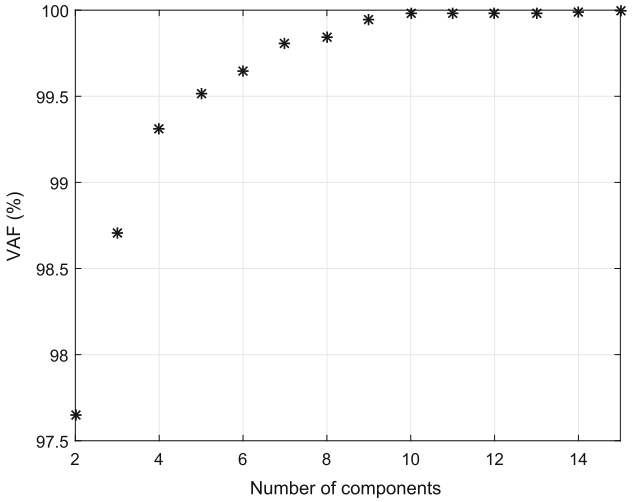


**Fig. 31** The efficiency of unobservable components, according to VAF criterion, for representing the experimental data of the daily deaths reports, in Brazil

of state variable $x_1$ consider operation regions with pre-established membership functions from expert knowledge, discarding any similarity degree from dynamic behavior of state variable $x_1$, which implies the increasing of filtering errors (Wang 1997; Babuska 1998; Sato-Ilic and Jain 2006).

On the other hand, the methodology for interval type-2 fuzzy Kalman filter design, proposed in this paper, considers the pre-processing of the noisy dynamic data of Lorenz chaotic attractor state variables, the computation of an interval adaptive similarity measure related to dynamic behavior of state variable $x_1$ resulting in membership functions with different formats and orientations for estimating regional models useful to characterize the dynamic behavior of Lorenz chaotic attractor. The adopted pre-processing method for fuzzy Kalman filter design is based on spectral decomposition of the noisy dynamic data of state variable $x_1$, resulting in unobservable spectral components with interpretable data patterns which allows to discard the spectral components associated with noise characteristic for better mathematical characterization of Lorenz chaotic attractor in the operation regions, recursively updated at each sampling time $k$, in order to reduce the filtering errors (Golyandina and Zhigljavsky 2013; Abdollahzade et al. 2015; Hossein and Saeid 2015; Juang 1994; Qi et al. 2019). For partitioning the dynamic data of state variable $x_1$ an interval adaptive similarity mechanism is adopted to define interval operation regions represented by interval membership functions, with different formats and orientations, adapted to the topological structure associated to the variability of dynamic data, in order to minimize the filtering errors (Babuska 1998; Höppner et al. 1999; Chaomurilige and Yang 2017).

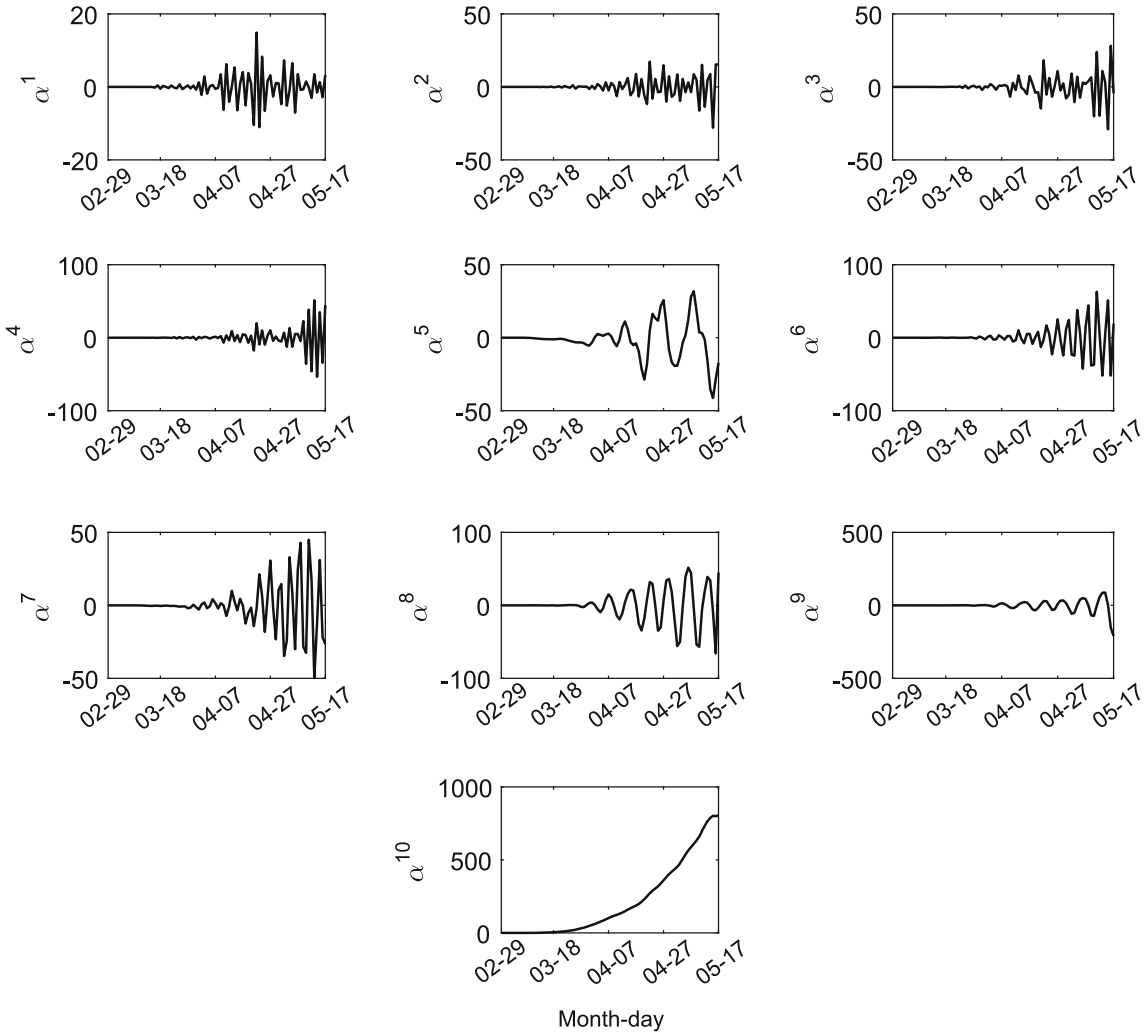


**Fig. 32** The temporal behavior of unobservable spectral components $\alpha^{j}|^{j=1,\ldots,10}$, which were extracted from experimental data of daily deaths, in Brazil

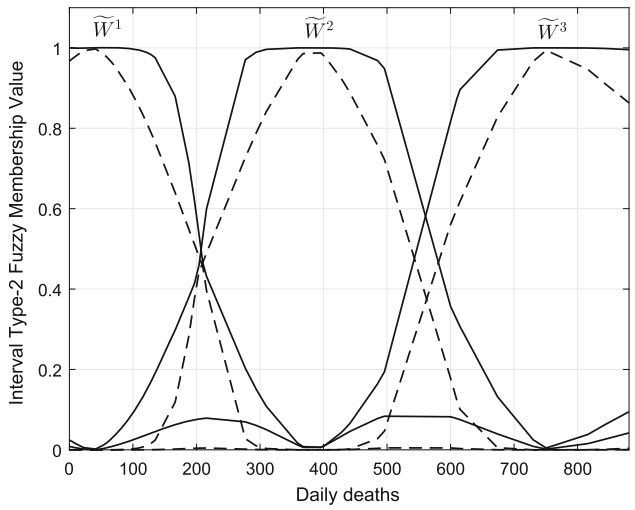


**Fig. 33** Interval type-2 fuzzy membership functions estimated from clustering of daily deaths reports, in Brazil

## 3.2 Experimental Results

In this section, experimental results for forecasting analysis of dynamic spread behavior taking into account the experimental data of daily deaths reports caused by COVID-19 in state of Maranhão and Brazil are presented.

### 3.2.1 Interval Type-2 Fuzzy Kalman Filtering and Forecasting Analysis of the Dynamic Spread of COVID-19 in State of Maranhão

The experimental data of daily deaths reports in the period ranging from 18 of March 2020 to 18 of May 2020 in state of Maranhão are shown in Fig. 17, which were obtained from the database provided by the State Health Organization of Maranhão[1]. Once that the problem of interest, in this paper,

[1] Available at: https://painel-covid19.saude.ma.gov.br/

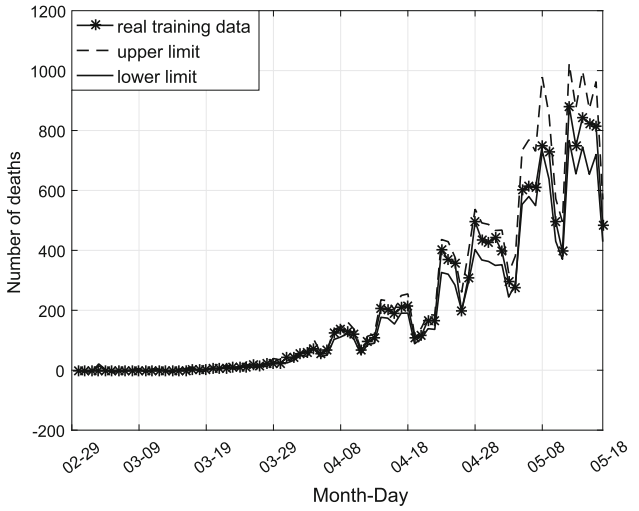


**Fig. 34** The confidence region generated by interval type-2 fuzzy Kalman filter for tracking the experimental data of daily deaths reports, from 29 of February 2020 to 18 of May 2020, in Brazil

is based on the time series related to daily deaths reports in state of Maranhão, the variable $\mathbf{u}_k$, in Eq. 15 of proposed methodology, is considered as white noise signal with low amplitude.

The pre-processing of experimental data by singular spectral analysis was able to extract the unobservable components associated to daily deaths reports. The variance accounted for (VAF) was considered as criterion for evaluating the appropriate number of these components, within a range from 2 to 15 ones, for best representation of the experimental data, as shown in Fig. 18. As it can be seen, considering the cost–benefit balance for computational practical application of the proposed methodology, the appropriated number of unobservable components was $\xi = 7$, with VAF value of 99.92% in efficiency to represent as accurately as possible the experimental data and, at same time, reducing the computational load of interval type-2 fuzzy Kalman filter algorithm. These spectral unobservable components, which were extracted from daily deaths reports in state of Maranhão, are shown in Fig. 19.

The partitions of experimental data related to daily deaths reports were defined by interval type-2 fuzzy Gustafson–Kessel clustering algorithm, as shown in Fig. 20, so the antecedent proposition, the rules number and consequent proposition, of the type-2 fuzzy Kalman filter, could be estimated successfully. For implementing the proposed type-2 fuzzy clustering algorithm, the following parameters were adopted: number of clusters $c = 3$, interval weighting exponent $\widetilde{m} = [2.0, 2.3]$ and termination tolerance $\mathcal{E} = 10^{-5}$.

The implementation of interval type-2 fuzzy OKID algorithm, for parametric estimation of consequent proposition in the type-2 fuzzy Kalman filter inference system, in Eq. 15, took into account the partitions on daily deaths reports, in Fig. 20, as weighting criterion, and the parameters values: $q = 1$, $\gamma = 5$ e $\beta = 5$. According to experimental data of daily deaths reports in state of Maranhão shown in Fig. 17, the pre-processed unobservable components shown in Fig. 19 and the interval type-2 fuzzy normalized membership values shown in Fig. 20, the initial parametric estimation of the type-2 fuzzy Kalman filter was computed by training step. The confidence region, as shown in Fig. 21, created by initial estimation of interval type-2 fuzzy Kalman filter taking into account uncertainties estimated by interval type-2 membership functions shown in Fig. 20, inherited to experimental data ranging from 18 of March 2020 to 18 of May 2020, illustrates its efficiency for tracking the experimental data of daily deaths reports in the state of Maranhão. From this confidence region, shown in Fig. 21, interval normal distribution projections were estimated, delimiting upper and lower limits for forecasting the future daily deaths reports in the state of Maranhão. The efficiency of interval type-2 fuzzy Kalman filter based on its initial estimation by training step from experimental data of daily deaths reports ranging from 18 of March 2020 to 18 of May 2020, for forecasting the future (validation) experimental data of daily deaths reports within the period ranging from 19 of May 2020 to 27 of May 2020, is shown in Fig. 22a. From 05 of May 2020 to 17 of May 2020, it was established a lockdown in metropolitan city of São Luís, and other four municipalities as well, in state of Maranhão, with positive reflexes on the numbers of confirmed cases and daily deaths reports. Due to this social context changing established by government in state of Maranhão, it was necessary a recursive updating of interval type-2 fuzzy Kalman filter on 24 of June 2020, for proposals of new tracking and forecasting future daily deaths reports within the period ranging from 25 of June 2020 to 03 of July 2020, as shown in Fig. 22b. The effect of lockdown can be observed within the period ranging from 28 of May 2020 to 01 of June 2020. The new recursive updating of the interval type-2 fuzzy Kalman filter was on 28 of July 2020, for proposals of new tracking and forecasting future daily deaths reports within the period ranging from 29 of July 2020 to 25 of August 2020, as shown in Fig. 22c. The new recursive updating of the interval type-2 fuzzy Kalman filter was on 25 of August 2020, for proposals of new tracking and forecasting future daily deaths reports within the period ranging from 26 of August 2020 to 25 of September 2020, as shown in Fig. 22d. The new recursive updating of the interval type-2 fuzzy Kalman filter was on 25 of September 2020, for proposals of new tracking and forecasting future daily deaths reports within the period ranging from 26 of September 2020 to ahead, as shown in Fig. 22e. It can be seen an efficiency in the adaptability of interval normal distribution projections created in real time by interval type-2 fuzzy Kalman filter, which illustrates its applicability for tracking and forecasting the COVID-19 dynamic spread experimental data related to

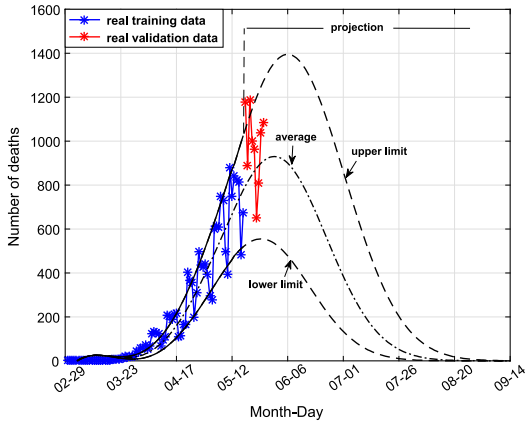


**(a)** The performance of interval type-2 fuzzy Kalman filter based on its initial estimation by training step for forecasting the future (validation) daily deaths reports within the period ranging from 29 of February 2020 to 18 of May 2020, in Brazil.

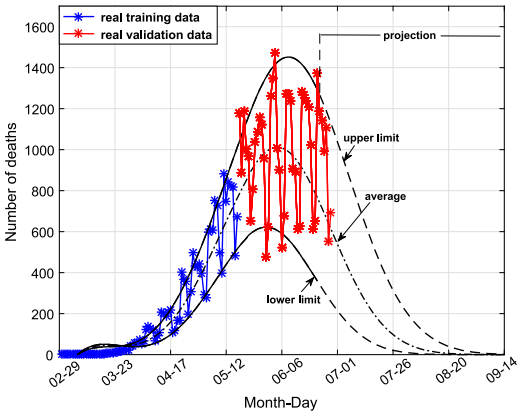


**(b)** The performance of interval type-2 fuzzy Kalman filter based on its recursive updating on 24 of June 2020 for forecasting the future (validation) daily deaths reports within the period ranging from 25 of June 2020 to 30 of June 2020, in Brazil.

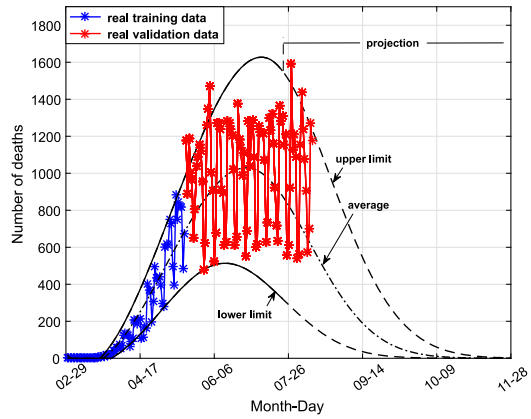


**(c)** The performance of interval type-2 fuzzy Kalman filter based on its recursive updating on 23 of July 2020 for forecasting the future (validation) daily deaths reports within the period ranging from 24 of July 2020 to 13 of August 2020, in Brazil.

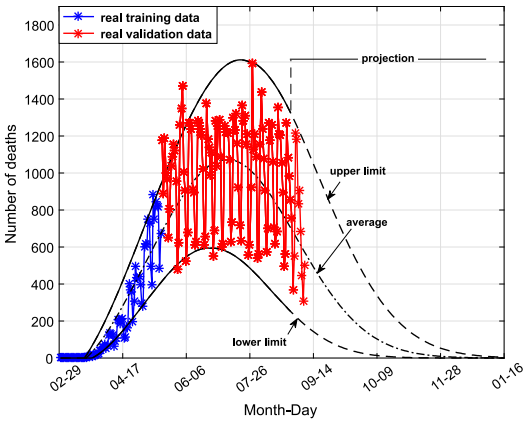


**(d)** The performance of interval type-2 fuzzy Kalman filter based on its recursive updating on 28 of August 2020 for forecasting the future (validation) daily deaths reports within the period ranging from 29 of August 2020 to 25 of September 2020, in Brazil.

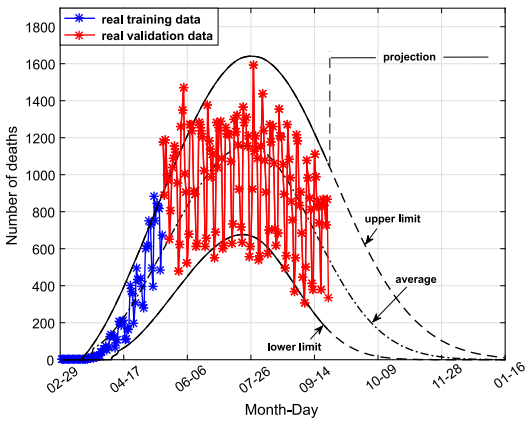


**(e)** The performance of interval type-2 fuzzy Kalman filter based on its recursive updating on 25 of September 2020 for forecasting the future (validation) daily deaths reports within the period ranging from 26 of September 2020 to ahead, in Brazil.

**Fig. 35** Performance of the interval type-2 fuzzy Kalman filter for tracking and forecasting the effects of COVID-19 spread experimental data related to daily deaths reports, in Brazil: **a** updating based on training data from 29 of February 2020 to 18 of May 2020; **b** recursive updating on 24 of June 2020; **c** recursive updating on 23 of July 2020; **d** recursive updating on 28 of August 2020; **e** recursive updating on 25 of September 2020

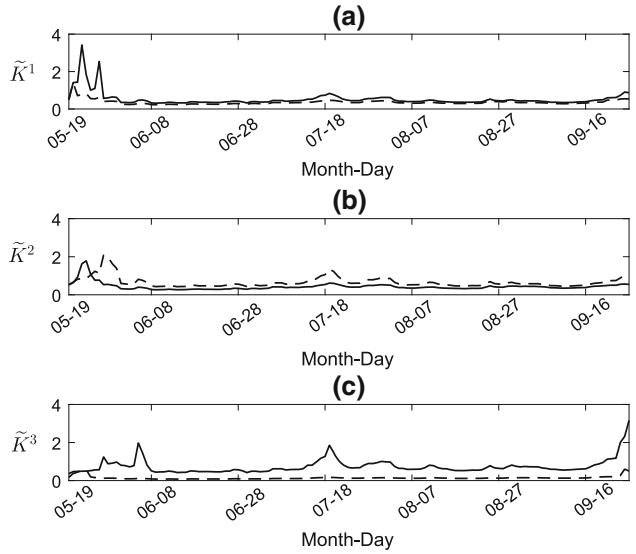


**Fig. 36** Interval type-2 fuzzy Kalman gains, during recursive updating of interval type-2 fuzzy Kalman filter for tracking and forecasting the COVID-19 dynamic spread experimental data related to daily deaths reports within period ranging from 19 of May 2020 to 25 of September, in Brazil: **a** Rule 1, **b** Rule 2, **c** Rule 3

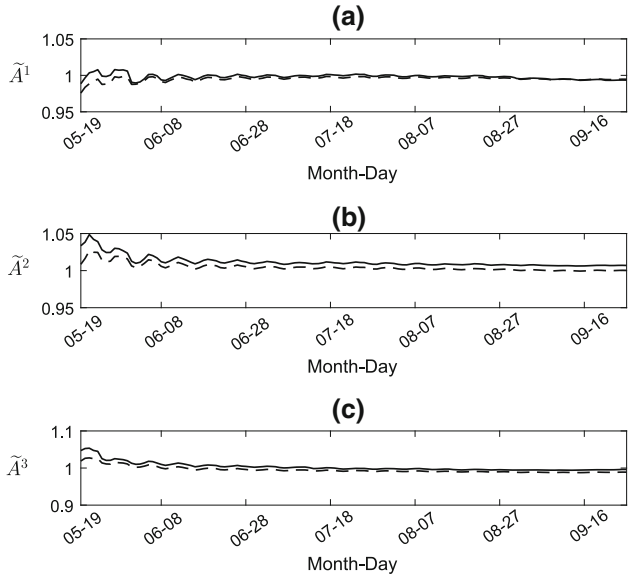


**Fig. 37** Interval type-2 fuzzy matrix $\widetilde{\mathbf{A}}^i$, during recursive updating of interval type-2 fuzzy Kalman filter for tracking and forecasting the COVID-19 dynamic spread experimental data related to daily deaths reports within period ranging from 19 of May 2020 to 25 of September, in Brazil: **a** Rule 1, **b** Rule 2, **c** Rule 3

daily deaths reports in state of Maranhão. The estimation of interval type-2 fuzzy Kalman gain matrices $\widetilde{\mathbf{K}}^i|^{i=1,\ldots,3}$, during recursive updating of interval type-2 fuzzy Kalman filter, within period ranging from 19 of May 2020 to 25 of September 2020, is shown in Fig. 23. The recursive estimation of the interval type-2 fuzzy matrices $\widetilde{\mathbf{A}}^i$, $\widetilde{\mathbf{B}}^i$, $\widetilde{\mathbf{C}}^i$ and $\widetilde{\mathbf{D}}^i$, with $i = 1, \ldots, 3$, in the consequent proposition of the interval type-2 fuzzy Kalman filter inference system, during recursive updating of interval type-2 fuzzy Kalman filter, within period ranging from 19 of May 2020 to 25 of September, is shown in Figs. 24, 25, 26, 27. The upper and lower instantaneous activation degrees related to interval type-2 fuzzy Kalman filter inference system, during its training and recursive step within period ranging from 18 of March 2020 to 25 of September, are shown in Fig. 28. The efficiency of interval type-2 fuzzy Kalman filter, during its recursive updating for tracking and forecasting the COVID-19 dynamic spread experimental data related to daily deaths reports in state of Maranhão, within period ranging from 19 of May 2020 to 29 of September, was validated through variance accounted for (VAF) criterion, as shown in Fig. 29.

According to results from real-time interval tracking and forecasting the COVID-19's dynamic spread behavior, based on experimental data of daily deaths reports, in state of Maranhão, the following auxiliary information and helpful for State Health Organization of Maranhão, it can be inferred that:

– The proposed methodology can be helpful to help the State Health Organization of Maranhão as auxiliary infor-

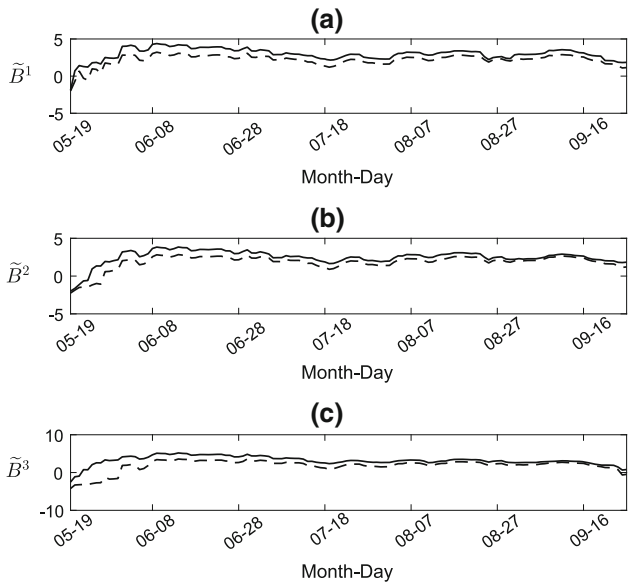


**Fig. 38** Interval type-2 fuzzy matrix $\widetilde{\mathbf{B}}^i$, during recursive updating of interval type-2 fuzzy Kalman filter for tracking and forecasting the COVID-19 dynamic spread experimental data related to daily deaths reports within period ranging from 19 of May 2020 to 25 of September, in Brazil: **a** Rule 1, **b** Rule 2, **c** Rule 3

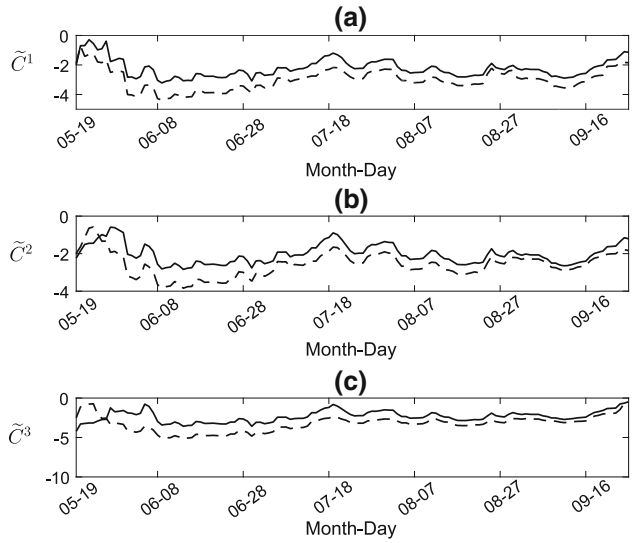


**Fig. 39** Interval type-2 fuzzy matrix $\widetilde{\mathbf{C}}^i$, during recursive updating of interval type-2 fuzzy Kalman filter for tracking and forecasting the COVID-19 dynamic spread experimental data related to daily deaths reports within period ranging from 19 of May 2020 to 25 of September, in Brazil: **a** Rule 1, **b** Rule 2, **c** Rule 3

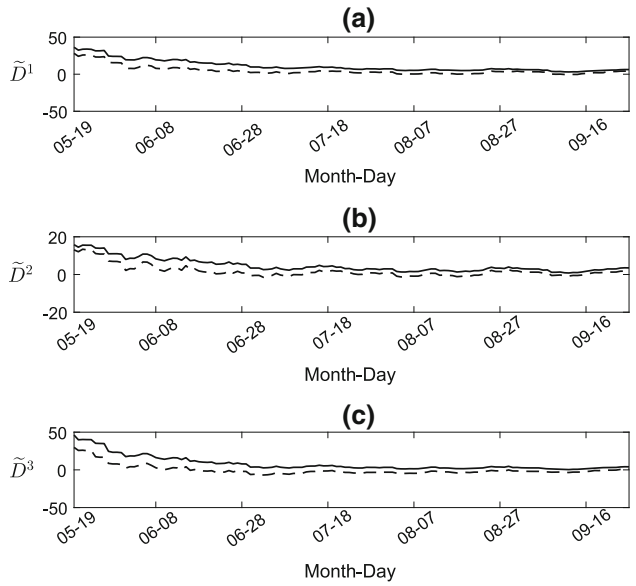


**Fig. 40** Interval type-2 fuzzy matrix $\widetilde{\mathbf{D}}^i$, during recursive updating of interval type-2 fuzzy Kalman filter for tracking and forecasting the COVID-19 dynamic spread experimental data related to daily deaths reports within period ranging from 19 of May 2020 to 25 of September, in Brazil: **a** Rule 1, **b** Rule 2, **c** Rule 3

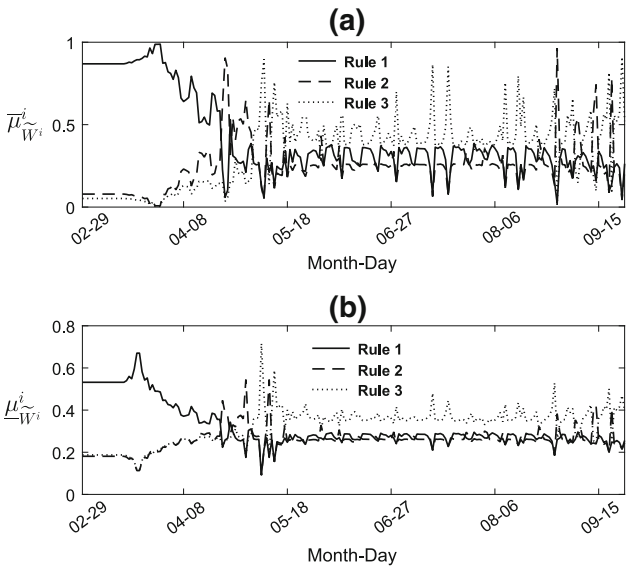


**Fig. 41** Instantaneous normalized fuzzy activation degrees of type-2 fuzzy Kalman inference system, during its recursive updating for tracking and forecasting the COVID-19 dynamic spread experimental data related to daily deaths reports within period ranging from 19 of May 2020 to 25 of September, in Brazil: **a** upper instantaneous normalized fuzzy activation degrees and **b** lower instantaneous normalized fuzzy activation degrees

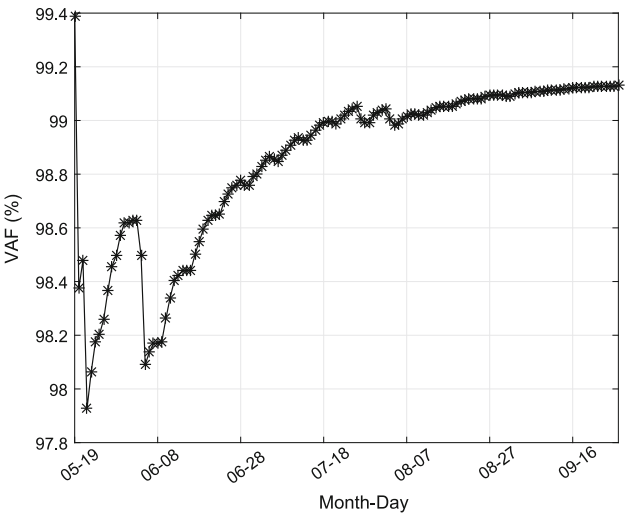


**Fig. 42** Real-time efficiency, based on VAF validation criterion, of interval type-2 fuzzy Kalman filter, during its recursive updating for tracking and forecasting the COVID-19 dynamic spread experimental data related to daily deaths reports within period ranging from 19 of May 2020 to 29 of September, in Brazil

mation in the diagnosis regarding the flexibility of social activities, in state of Maranhão. Figure 22 depicts a time-based displacement of the interval projections as well as their amplitudes, as the daily deaths reports are processed by interval type-2 fuzzy Kalman filter. From the recursive updating on 25 of September 2020, the forecasting interval projections indicate the month of November as more adequate for reevaluating the requirements on flexibility of social activities, in state of Maranhão.

### 3.2.2 Interval Type-2 Fuzzy Kalman Filtering and Forecasting Analysis of the Dynamic Spread of COVID-19 in Brazil

The experimental data corresponding to daily deaths reports within the period ranging from 29 of February 2020 to 18 of May 2020, in Brazil, are shown in Fig. 30, which were extracted from official report by Ministry of Health of Brazil[2]. Once that the problem of interest, in this paper, is based on the time series related to daily deaths reports in Brazil, the variable $\mathbf{u}_k$, in Eq. 15 of proposed methodology, is considered as white noise signal with low amplitude.

The pre-processing of experimental data by singular spectral analysis was able to extract the unobservable components associated to daily deaths reports. The variance accounted for (VAF) was considered as criterion for evaluating the appropriate number of these components, within a range from 2 to 15 ones, for best representation of the experimental data, as shown in Fig. 31. As it can be seen, considering the cost–benefit balance for computational practical application of the proposed methodology, the appropriated number of unobservable components was $\xi = 10$, with VAF value of 99.98% in efficiency to represent as accurately as possible the experimental data and, at same time, reducing the computational load of interval type-2 fuzzy Kalman filter algorithm. These spectral unobservable components, which were extracted from daily deaths reports in Brazil, are shown in Fig. 32.

The partitions of experimental data related to daily deaths reports were defined by interval type-2 fuzzy Gustafson–Kessel clustering algorithm, as shown in Fig. 33, so the antecedent proposition, the rules number and consequent proposition, of the type-2 fuzzy Kalman filter, could be estimated successfully. For implementing the proposed type-2 fuzzy clustering algorithm, the following parameters were adopted: number of clusters $c = 3$, interval weighting exponent $\widetilde{m} = [1.5, 2.3]$ and termination tolerance $\mathcal{E} = 10^{-5}$.

The implementation of interval type-2 fuzzy OKID algorithm, for parametric estimation of consequent proposition in the type-2 fuzzy Kalman filter inference system, in Eq. 15, took into account the partitions on daily deaths reports, in Fig 33, as weighting criterion, and the parameters values: $q = 1$, $\gamma = 15$ e $\beta = 15$. According to experimental data of daily deaths reports in Brazil shown in Fig. 30, the pre-processed unobservable components shown in Fig. 32 and the interval type-2 fuzzy normalized membership values shown in Fig. 33, the initial parametric estimation of the type-2 fuzzy Kalman filter was computed by training step. The confidence region, as shown in Fig. 34, created by initial estimation of interval type-2 fuzzy Kalman filter taking into account uncertainties estimated by interval type-2 membership functions shown in Fig. 33, inherited to experimental data ranging from 29 of February 2020 to 18 of May 2020, illustrates its efficiency for tracking the experimental data of daily deaths reports in Brazil.

From this confidence region, shown in Fig. 34, interval normal distribution projections were estimated, delimiting upper and lower limits for forecasting the future daily deaths reports in Brazil. The efficiency of interval type-2 fuzzy Kalman filter based on its initial estimation by training step from experimental data of daily deaths reports ranging from 29 of February 2020 to 18 of May 2020, for forecasting the future (validation) experimental data of daily deaths reports within the period ranging from 19 of May 2020 to 27 of May 2020, is shown in Fig. 35a. The new recursive updating of interval type-2 fuzzy Kalman filter on 24 of June 2020, for proposals of new tracking and forecasting future daily deaths reports within the period ranging from 25 of June 2020 to 30 of June 2020, is shown in Fig. 35b. The new recursive updating of the interval type-2 fuzzy Kalman filter was on 23 of July 2020, for proposals of new tracking and forecasting future daily deaths reports within the period ranging from 24 of July 2020 to 13 of August 2020, as shown in Fig. 35c. The new recursive updating of the interval type-2 fuzzy Kalman filter was on 28 of August 2020, for proposals of new tracking and forecasting future daily deaths reports within the period ranging from 29 of August 2020 to 25 of September 2020, as shown in Fig. 35d. The new recursive updating of the interval type-2 fuzzy Kalman filter was on 25 of September 2020, for proposals of new tracking and forecasting future daily deaths reports within the period ranging from 26 of September 2020 to ahead, as shown in Fig. 35e. It can be seen an efficiency in the adaptability of interval normal distribution projections created in real time by interval type-2 fuzzy Kalman filter, which illustrates its applicability for tracking and forecasting the COVID-19 dynamic spread experimental data related to daily deaths reports in Brazil. The estimation of interval type-2 fuzzy Kalman gain matrices $\widetilde{\mathbf{K}}^i|^{i=1,\ldots,3}$, during recursive updating of interval type-2 fuzzy Kalman filter, within period ranging from 19 of May 2020 to 25 of September, in Brazil, is shown in Fig. 36. The recursive estimations of the interval type-2 fuzzy matrices $\widetilde{\mathbf{A}}^i$, $\widetilde{\mathbf{B}}^i$, $\widetilde{\mathbf{C}}^i$ and $\widetilde{\mathbf{D}}^i$, with $i = 1, \ldots, 3$, in the consequent proposition of the interval type-2 fuzzy Kalman filter inference system, during recursive updating of interval type-2 fuzzy Kalman filter, within period ranging from 19 of May 2020 to 25 of September, are shown in Figs. 37, 38, 39, 40. The upper and lower instantaneous activation degrees related to interval type-2 fuzzy Kalman filter inference system, during its training and recursive step within period ranging from 29 of February 2020 to 25 of September, in Brazil, are shown in Fig. 41. The efficiency of interval type-2 fuzzy Kalman filter, during its recursive updating for tracking and forecasting the COVID-19 dynamic spread experimental data related to daily

[2] Available at: https://covid.saude.gov.br/

deaths reports within period ranging from 19 of May 2020 to 29 of September, in Brazil, was validated through Variance Accounted For (VAF) criterion, as shown in Fig. 42.

According to results from real-time interval tracking and forecasting the COVID-19's dynamic spread behavior, based on experimental data of daily deaths reports, in Brazil, the following auxiliary information, and helpful for Ministry of Health of Brazil, it can be inferred that:

– The proposed methodology can be helpful to help the Ministry of Health of Brazil as auxiliary information in the diagnosis regarding the flexibility of social activities, in Brazil. Figure 35 depicts a time-based displacement of the interval projections as well as their amplitudes, as the daily deaths reports are processed by interval type-2 fuzzy Kalman filter. From the recursive updating on 25 of September, the forecasting interval projections indicate the month of January 2021 as more adequate for reevaluating the requirements on flexibility of social activities, in Brazil.

## 4 Conclusion

In this paper, an approach for experimental data-based design of interval type-2 fuzzy Kalman filters was proposed. The computational results showed efficiency of designed interval type-2 fuzzy Kalman filter, due to its spectral pre-processing analysis mechanism, for filtering and tracking data set of Lorenz's chaotic attractor in a noisy environment, as compared to another approach widely cited in the literature. The experimental results showed the applicability of designed interval type-2 fuzzy Kalman filter, due to its recursive updating mechanism, for adaptive and real-time forecasting the COVID-19 spread dynamics related to daily deaths reports in state of Maranhão and Brazil.

From the recursive updating on 25 of September 2020, it could be inferred by forecasting interval projections the month of January 2021 as more adequate for reassessment the requirements on flexibility of social activities in Brazil (containing the 27 states and federal district) and the month of November as more adequate for reassessment the requirements on flexibility of social activities in state of Maranhão.

For further works, the formulation and applicability of proposed methodology in the context of evolving interval type-2 fuzzy systems are of particular interest.

**Acknowledgements** This work was developed in the Laboratory of Computational Intelligence Applied to Technology at Federal Institute of Education, Science and Technology of Maranhão. The authors are grateful to Coordination for the Improvement of Higher Education Personnel (CAPES) for financial support and to the Master and Doctorate Program in Electrical Engineering at Federal University of Maranhão (PPGEE-UFMA) for their support in the development of this research.

## References

(2020a) Controlling the spread of covid-19 at ground crossings. Tech. rep., World Health Organization, https://www.who.int/

(2020b) Infection prevention and control for the safe management of a dead body in the context of covid-19: interim guidance. Tech. rep., World Health Organization, https://www.who.int/

Abdollahzade, M., ArashMiranian, Hassani, H., & HosseinIranmanesh, (2015). A new hybrid enhanced local linear neuro-fuzzy model based on the optimized singular spectrum analysis and its application for nonlinear and chaotic time series forecasting. *Information Sciences,*. https://doi.org/10.1016/j.ins.2014.09.002.

Antsaklis, P. J., & Liu, D. (2003). *Stability and control of dynamical systems with applications*. Basel: Birkhäuser.

Asl, R. M., Palm, R., Wu, H., & Handroos, H. (2020). Fuzzy-based parameter optimization of adaptive unscented kalman filter: Methodology and experimental validation. *IEEE Access*, *8*, 54887–54904. https://doi.org/10.1109/access.2020.2979987.

Babuska, R. (1998). *Fuzzy modeling for control*. New York: Springer.

Benhamida, I., Ameur, A., Kouzi, K., & Gaoui, B. (2019). Torque ripple minimization in predictive torque control method of PMSM drive using adaptive fuzzy logic modulator and EKF estimator. *Journal of Control, Automation and Electrical Systems*, *30*(6), 1007–1018. https://doi.org/10.1007/s40313-019-00505-7.

Bouhentala, M., Ghanai, M., & Chafaa, K. (2019). Interval-valued membership function estimation for fuzzy modeling. *Fuzzy Sets and Systems*, *361*, 101–113. https://doi.org/10.1016/j.fss.2018.06.008.

Brown, S. M., Peltan, I. D., Webb, B., Kumar, N., Starr, N., Grissom, C., et al. (2020). Hydroxychloroquine vs. azithromycin for hospitalized patients with suspected or confirmed COVID-19 (HAHPS): Protocol for a pragmatic, open label, active comparator trial. *Annals of the American Thoracic Society*. https://doi.org/10.1513/annalsats.202004-309sd.

Chakraborty, I., & Maity, P. (2020). COVID-19 outbreak: Migration, effects on society, global environment and prevention. *Science of The Total Environment*, *728*, 138882. https://doi.org/10.1016/j.scitotenv.2020.138882.

Chaomurilige, Yu J, & Yang, M. S. (2017). Deterministic annealing gustafson-kessel fuzzy clustering algorithm. *Information Sciences*, *417*, 435–453. https://doi.org/10.1016/j.ins.2017.07.005.

Chen, C. T. (1999). *Linear system theory and design*. Oxford: Oxford University Press.

Chen, Y., Leng, K., Lu, Y., Wen, L., Qi, Y., Gao, W., et al. (2020). Epidemiological features and time-series analysis of influenza incidence in urban and rural areas of shenyang, china, 2010–2018. *Epidemiology and Infection*, *148*, https://doi.org/10.1017/s0950268820000151.

Chin, C. S., & Lin, W. P. (2018). Robust genetic algorithm and fuzzy inference mechanism embedded in a sliding-mode controller for an uncertain underwater robot. *IEEE/ASME Transactions on Mechatronics*, *23*(2), 655–666. https://doi.org/10.1109/tmech.2018.2806389.

Chintalapudi, N., Battineni, G., & Amenta, F. (2020). COVID-19 virus outbreak forecasting of registered and recovered cases after sixty day lockdown in italy: A data driven model approach. *Journal of Microbiology, Immunology and Infection*, *53*(3), 396–403. https://doi.org/10.1016/j.jmii.2020.04.004.

Chowell, G., Luo, R., Sun, K., Roosa, K., Tariq, A., & Viboud, C. (2020). Real-time forecasting of epidemic trajectories using computational dynamic ensembles. *Epidemics*, *30*, 100379. https://doi.org/10.1016/j.epidem.2019.100379.

Deeba, F., Haider, M. S. H., Ahmed, A., Tazeen, A., Faizan, M. I., Salam, N., et al. (2020). Global transmission and evolutionary dynamics of the chikungunya virus. *Epidemiology and Infection*, *148*, https://doi.org/10.1017/s0950268820000497.

Duan, X., & Zhang, X. (2020). ARIMA modelling and forecasting of irregularly patterned COVID-19 outbreaks using japanese and south korean data. *Data in Brief*, *31*, 105779. https://doi.org/10.1016/j.dib.2020.105779.

Elsner, J. B. (2002). Analysis of time series structure: SSA and related techniques. *Journal of the American Statistical Association*, *97*(460), 1207–1208. https://doi.org/10.1198/jasa.2002.s239.

Evangelista, A. P. F., & Serra, G. L. O. (2019). Multivariable state-space recursive identification algorithm based on evolving type-2 neural-fuzzy inference system. *Journal of Control, Automation and Electrical Systems*, *30*(6), 921–942. https://doi.org/10.1007/s40313-019-00528-0.

Eyoh, I., John, R., Maere, G. D., & Kayacan, E. (2018). Hybrid learning for interval type-2 intuitionistic fuzzy logic systems as applied to identification and prediction problems. *IEEE Transactions on Fuzzy Systems*, *26*(5), 2672–2685. https://doi.org/10.1109/tfuzz.2018.2803751.

Feng, Y., Ling, Y., Bai, T., Xie, Y., Huang, J., Li, J., et al. (2020). COVID-19 with different severities: A multicenter study of clinical features. *American Journal of Respiratory and Critical Care Medicine*, *201*(11), 1380–1388. https://doi.org/10.1164/rccm.202002-0445oc.

Fishbane, S., & Hirsch, J. S. (2020). Erythropoiesis-stimulating agent treatment in patients with COVID-19. *American Journal of Kidney Diseases*,. https://doi.org/10.1053/j.ajkd.2020.05.002.

Franklin, G. F., Powell, J. D., & Workman, M. L. (1997). *Digital Control of Dynamic Systems*. New York: Addison-Wesley Publishing Company.

Fredj, H. B., & Chrif, F. (2020). Novel corona virus disease infection in tunisia: Mathematical model and the impact of the quarantine strategy. *Chaos, Solitons & Fractals*, 109969. https://doi.org/10.1016/j.chaos.2020.109969.

Gil, P., Oliveira, T., & Palma, L. (2019). Adaptive neuro–fuzzy control for discrete-time nonaffine nonlinear systems. *IEEE Transactions on Fuzzy Systems*, *27*(8), 1602–1615. https://doi.org/10.1109/tfuzz.2018.2883540.

Golyandina, N., & Zhigljavsky, A. (2013). Singular spectrum analysis for time series. https://doi.org/10.1007/978-3-642-34913-3.

Gomez-Garcia, R., Yang, L., Munoz-Ferreras, J. M., & Feng, W. (2020). Lossy signal-interference filters and applications. *IEEE Transactions on Microwave Theory and Techniques*, *68*(2), 516–529. https://doi.org/10.1109/tmtt.2019.2953585.

He, D., Wang, X., Gao, D., & Wang, J. (2018). Modeling the 2016–2017 yemen cholera outbreak with the impact of limited medical resources. *Journal of Theoretical Biology*, *451*, 80–85. https://doi.org/10.1016/j.jtbi.2018.04.041.

Hossein, Hassani, & Saeid, Sanei. (2015). *Singular spectrum analysis of biomedical signals*. New York: Taylor & Francis Ltd.

Hranac, C. R., Marshall, J. C., Monadjem, A., & Hayman, D. T. (2019). Predicting ebola virus disease risk and the role of african bat birthing. *Epidemics*, *29*, 100366. https://doi.org/10.1016/j.epidem.2019.100366.

Huang, Y., Zhang, P., & Zhao, W. (2015). Novel grid multiwing butterfly chaotic attractors and their circuit design. *IEEE Transactions on Circuits and Systems II: Express Briefs*, *62*(5), 496–500. https://doi.org/10.1109/tcsii.2014.2385274.

Huang, Y., Chen, S., Yang, Z., Guan, W., Liu, D., Lin, Z., et al. (2020). SARS-CoV-2 viral load in clinical samples from critically ill patients. *American Journal of Respiratory and Critical Care Medicine*, *201*(11), 1435–1438. https://doi.org/10.1164/rccm.202003-0572le.

Hwang, C. L., Wu, H. M., & Lai, J. Y. (2019). On-line obstacle detection, avoidance, and mapping of an outdoor quadrotor using EKF-based fuzzy tracking incremental control. *IEEE Access*, *7*, 160203–160216. https://doi.org/10.1109/access.2019.2950324.

Höppner, F., Klawonn, F., Kruse, R., & Runkler, T. (1999). *Fuzzy cluster analysis: methods for classification, data analysis and image recognition*. New York: Wiley.

Juang, J. N. (1994). *Applied system identification*. New Jersey: Prentice Hall.

Kalman, R. E. (1960). A new approach to linear filtering and prediction problems. *Journal of Basic Engineering*, *82*(1), 35–45. https://doi.org/10.1115/1.3662552.

Kanagarathinam, K., & Sekar, K. (2020). Estimation of reproduction number (ro) and early prediction of 2019 novel coronavirus disease (COVID-19) outbreak in india using statistical computing approach. *Epidemiology and Health*, e2020028. https://doi.org/10.4178/epih.e2020028.

Kang, H., Xia, L., Yan, F., Wan, Z., Shi, F., Yuan, H., et al. (2020). Diagnosis of coronavirus disease 2019 (COVID-19) with structured latent multi-view representation learning. *IEEE Transactions on Medical Imaging*, 1–1. https://doi.org/10.1109/tmi.2020.2992546.

van de Kassteele, J., Eilers, P. H. C., & Wallinga, J. (2019). Nowcasting the number of new symptomatic cases during infectious disease outbreaks using constrained p-spline smoothing. *Epidemiology*, *30*(5), 737–745. https://doi.org/10.1097/ede.0000000000001050.

Khodaei-Mehr, J., Tangestanizadeh, S., Vatankhah, R., & Sharifi, M. (2018). Optimal neuro-fuzzy control of hepatitis c virus integrated by genetic algorithm. *IET Systems Biology*, *12*(4), 154–161. https://doi.org/10.1049/iet-syb.2017.0074.

Kim, H. J., Park, J. B., & Joo, Y. H. (2020a). Decentralized $h_\infty$ sampled-data fuzzy filter for nonlinear interconnected oscillating systems with uncertain interconnections. *IEEE Transactions on Fuzzy Systems*, *28*(3), 487–498. https://doi.org/10.1109/tfuzz.2019.2908151.

Kim, S., Seo, Y. B., & Jung, E. (2020b). Prediction of COVID-19 transmission dynamics using a mathematical model considering behavior changes. *Epidemiology and Health*, e2020026. https://doi.org/10.4178/epih.e2020026.

Koolhof, I. S., Gibney, K. B., Bettiol, S., Charleston, M., Wiethoelter, A., Arnold, A. L., et al. (2020). The forecasting of dynamical ROSS river virus outbreaks: Victoria, Australia. *Epidemics*, *30*, 100377. https://doi.org/10.1016/j.epidem.2019.100377.

Korcinska, M. R., Bjerre, K. D., Rasmussen, L. D., Jensen, E. T., Fischer, T. K., Barrasa, A., et al. (2020). Detection of norovirus infections in denmark, 2011–2018. *Epidemiology and Infection*, *148*, https://doi.org/10.1017/s0950268820000461.

Liang, Q., & Mendel, J. (2000). Interval type-2 fuzzy logic systems: theory and design. *IEEE Transactions on Fuzzy Systems*, *8*(5), 535–550. https://doi.org/10.1109/91.873577.

Lin, Q., Zhao, S., Gao, D., Lou, Y., Yang, S., Musa, S. S., et al. (2020). A conceptual model for the coronavirus disease 2019 (COVID-19) outbreak in wuhan, china with individual reaction and governmental action. *International Journal of Infectious Diseases*, *93*, 211–216. https://doi.org/10.1016/j.ijid.2020.02.058.

Liu, W., Liu, Y., & Bucknall, R. (2019). A robust localization method for unmanned surface vehicle (USV) navigation using fuzzy adaptive kalman filtering. *IEEE Access*, *7*, 46071–46083. https://doi.org/10.1109/access.2019.2909151.

Luenberger, D. G. (1979). *Introduction to dynamic systems: theory, models, and applications*. New York: Wiley.

Mack, W., & Habets, E. A. P. (2020). Deep filtering: Signal extraction and reconstruction using complex time-frequency filters. *IEEE Signal Processing Letters*, *27*, 61–65. https://doi.org/10.1109/lsp.2019.2955818.

Martins, D. P., Barros, M. T., Pierobon, M., Kandhavelu, M., Lio, P., & Balasubramaniam, S. (2018). Computational models for trapping ebola virus using engineered bacteria. *IEEE/ACM Transactions on Computational Biology and Bioinformatics*, *15*(6), 2017–2027. https://doi.org/10.1109/tcbb.2018.2836430.

Matía, F., Jiménez, V., Alvarado, B. P., & Haber, R. (2019). The fuzzy kalman filter: Improving its implementation by reformulating uncertainty representation. *Fuzzy Sets and Systems*,. https://doi.org/10.1016/j.fss.2019.10.015.

Mendel, J. M. (2019). Comparing the performance potentials of interval and general type-2 rule-based fuzzy systems in terms of sculpting the state space. *IEEE Transactions on Fuzzy Systems*, *27*(1), 58–71. https://doi.org/10.1109/tfuzz.2018.2856184.

Mohd, M. H., & Sulayman, F. (2020). Unravelling the myths of r0 in controlling the dynamics of COVID-19 outbreak: A modelling perspective. *Chaos, Solitons & Fractals*, *138*, 109943. https://doi.org/10.1016/j.chaos.2020.109943.

Páramo-Carranza, L. A., Meda-Campaña, J. A., de Jesús, Rubio J., Tapia-Herrera, R., Curtidor-López, A. V., Grande-Meza, A., et al. (2017). Discrete-time kalman filter for takagi–sugeno fuzzy models. *Evolving Systems*, *8*(3), 211–219. https://doi.org/10.1007/s12530-017-9181-0.

Park, S. W., Cornforth, D. M., Dushoff, J., & Weitz, J. S. (2020). The time scale of asymptomatic transmission affects estimates of epidemic potential in the COVID-19 outbreak. *Epidemics*, *31*, 100392. https://doi.org/10.1016/j.epidem.2020.100392.

Pham, T. D., & Berger, K. (2011). Automated detection of white matter changes in elderly people using fuzzy, geostatistical, and information combining models. *IEEE Transactions on Information Technology in Biomedicine*, *15*(2), 242–250. https://doi.org/10.1109/titb.2010.2081996.

Pires, D. S., & Serra, G. L. O. (2019). Methodology for evolving fuzzy kalman filter identification. *International Journal of Control, Automation and Systems*, *17*(3), 793–800. https://doi.org/10.1007/s12555-017-0503-6.

Price, O. H., Sullivan, S. G., Sutterby, C., Druce, J., & Carville, K. S. (2019). Using routine testing data to understand circulation patterns of influenza a, respiratory syncytial virus and other respiratory viruses in victoria, australia. *Epidemiology and Infection*, *147*, https://doi.org/10.1017/s0950268819001055.

Qi, R., Tao, G., & Jiang, B. (2019). Fuzzy system identification and adaptive control. https://doi.org/10.1007/978-3-030-19882-4.

Rajaei, A., Vahidi-Moghaddam, A., Chizfahm, A., & Sharifi, M. (2019). Control of malaria outbreak using a non-linear robust strategy with adaptive gains. *IET Control Theory & Applications*, *13*(14), 2308–2317. https://doi.org/10.1049/iet-cta.2018.5292.

Rustam, F., Reshi, A. A., Mehmood, A., Ullah, S., On, B., Aslam, W., et al. (2020). COVID-19 future forecasting using supervised machine learning models. *IEEE Access*, 1–1. https://doi.org/10.1109/access.2020.2997311.

Ryu, S., & Chun, B. C. (2020). An interim review of the epidemiological characteristics of 2019 novel coronavirus. *Epidemiology and Health*, *42*, e2020006. https://doi.org/10.4178/epih.e2020006.

Sato-Ilic, M., & Jain, L. C. (2006). *Innovations in fuzzy clustering: theory and applications*. New York: Springer.

Serra, G. L. O. (Ed.). (2012). Frontiers in advanced control systems. InTech. https://doi.org/10.5772/1267.

Serra, G. L. O. (Ed.). (2018). Kalman filters: Theory for advanced applications. InTech. https://doi.org/10.5772/intechopen.68249.

Sloan, C., Chandrasekhar, R., Mitchel, E., Ndi, D., Miller, L., Thomas, A., et al. (2020). Spatial and temporal clustering of patients hospitalized with laboratory-confirmed influenza in the united states. *Epidemics*, *31*, 100387. https://doi.org/10.1016/j.epidem.2020.100387.

Stocks, T., Martin, L. J., Kühlmann-Berenzon, S., & Britton, T. (2020). Dynamic modeling of hepatitis c transmission among people who inject drugs. *Epidemics*, *30*, 100378. https://doi.org/10.1016/j.epidem.2019.100378.

Sun, N., Wei, L., Shi, S., Jiao, D., Song, R., Ma, L., et al. (2020). A qualitative study on the psychological experience of caregivers of COVID-19 patients. *American Journal of Infection Control*, *48*(6), 592–598. https://doi.org/10.1016/j.ajic.2020.03.018.

van Gaalen, R. D., van de Kassteele, J., Hahné, S. J. M., Bruijning-Verhagen, P., & Wallinga, J. (2017). Determinants of rotavirus transmission. *Epidemiology*, *28*(4), 503–513. https://doi.org/10.1097/ede.0000000000000654.

Wang, L. X. (1997). *A course in fuzzy systems and control*. Upper Saddle River: Prentive-Hall Intervational, Inc.

Wang, X., Xu, Z., Gou, X., & Trajkovic, L. (2020). Tracking a maneuvering target by multiple sensors using extended kalman filter with nested probabilistic-numerical linguistic information. *IEEE Transactions on Fuzzy Systems*, *28*(2), 346–360. https://doi.org/10.1109/tfuzz.2019.2906577.

Wang, Z. P., & Wu, H. N. (2019). Robust guaranteed cost sampled-data fuzzy control for uncertain nonlinear time-delay systems. *IEEE Transactions on Systems, Man, and Cybernetics: Systems*, *49*(5), 964–975. https://doi.org/10.1109/tsmc.2017.2703837.

Watkins, N. J., Nowzari, C., & Pappas, G. J. (2020). Robust economic model predictive control of continuous-time epidemic processes. *IEEE Transactions on Automatic Control*, *65*(3), 1116–1131. https://doi.org/10.1109/tac.2019.2919136.

Weng, R. X., Fu, H. L., Zhang, C. L., Ye, J. B., Hong, F. C., Chen, X. S., et al. (2020). Time series analysis and forecasting of chlamydia trachomatis incidence using surveillance data from 2008 to 2019 in shenzhen, china. *Epidemiology and Infection*, https://doi.org/10.1017/s0950268820000680.

Yang, S., Deng, B., Wang, J., Liu, C., Li, H., Lin, Q., et al. (2019). Design of hidden-property-based variable universe fuzzy control for movement disorders and its efficient reconfigurable implementation. *IEEE Transactions on Fuzzy Systems*, *27*(2), 304–318. https://doi.org/10.1109/tfuzz.2018.2856182.

Zhao, J., & Lin, C. M. (2019). Wavelet-TSK-type fuzzy cerebellar model neural network for uncertain nonlinear systems. *IEEE Transactions on Fuzzy Systems*, *27*(3), 549–558. https://doi.org/10.1109/tfuzz.2018.2863650.

Zhong, L., Mu, L., Li, J., Wang, J., Yin, Z., & Liu, D. (2020). Early prediction of the 2019 novel coronavirus outbreak in the mainland china based on simple mathematical model. *IEEE Access*, *8*, 51761–51769. https://doi.org/10.1109/access.2020.2979599.

Zhu, X., Wang, T., Bao, Y., Hu, F., & Li, S. (2019). Signal detection in generalized gaussian distribution noise with nakagami fading channel. *IEEE Access*, *7*, 23120–23126. https://doi.org/10.1109/access.2019.2895627.